nature communications

Article

https://doi.org/10.1038/s41467-024-52812-6

Spatiotemporal control of neutrophil fate to tune inflammation and repair for myocardial infarction therapy

Received: 15 February 2024

Accepted: 23 September 2024

Published online: 01 October 2024

Check for updates

Cheesue Kim[1,11], Hyeok Kim[2,3,11], Woo-Sup Sim[2,3,11], Mungyo Jung[1], Jihye Hong[4], Sangjun Moon[1], Jae-Hyun Park[2,3], Jin-Ju Kim[2,3], Mikyung Kang[5], Sungpil Kwon[1], Mi-Jeong Kim[3], Kiwon Ban[6], Hun-Jun Park[2,3,7] ✉ & Byung-Soo Kim[1,4,8,9,10] ✉

Neutrophils are critical mediators of both the initiation and resolution of inflammation after myocardial infarction (MI). Overexuberant neutrophil signaling after MI exacerbates cardiomyocyte apoptosis and cardiac remodeling while neutrophil apoptosis at the injury site promotes macrophage polarization toward a pro-resolving phenotype. Here, we describe a nanoparticle that provides spatiotemporal control over neutrophil fate to both stymie MI pathogenesis and promote healing. Intravenous injection of roscovitine/catalase-loaded poly(lactic-co-glycolic acid) nanoparticles after MI leads to nanoparticle uptake by circulating neutrophils migrating to the infarcted heart. Activated neutrophils at the infarcted heart generate reactive oxygen species, triggering intracellular release of roscovitine, a cyclin-dependent kinase inhibitor, from the nanoparticles, thereby inducing neutrophil apoptosis. Timely apoptosis of activated neutrophils at the infarcted heart limits neutrophil-driven inflammation, promotes macrophage polarization toward a pro-resolving phenotype, and preserves heart function. Modulating neutrophil fate to tune both inflammatory and reparatory processes may be an effective strategy to treat MI.

Myocardial infarction (MI) is one of the leading causes of morbidity worldwide[1,2]. Neutrophils are short-lived immune cells that play critical roles in initiating both the inflammatory and reparatory processes following MI[3–5]. Neutrophils migrate to the heart shortly after MI in response to damage-associated molecular patterns (DAMPs) and other inflammatory cues released by dying cardiac cells[6]. Upon arrival, neutrophils are activated by reactive oxygen species (ROS)-dependent pathways to secrete pro-inflammatory cytokines, chemokines, proteases, and neutrophil extracellular traps (NETs)[5–7], which incite cardiomyocyte death and tissue damage[8,9] and amplify the inflammatory cascade through pro-inflammatory macrophage polarization[10–12]. While cardiac neutrophil activation is crucial for the initiation of the inflammatory cascade post-MI, cardiac neutrophil death, particularly through the immunologically silent process of apoptosis, is

[1]School of Chemical and Biological Engineering, Seoul National University, Seoul, Republic of Korea. [2]Department of Biomedicine & Health Sciences, The Catholic University of Korea, Seoul, Republic of Korea. [3]Department of Internal Medicine, Seoul Saint Mary's Hospital, Seoul, Republic of Korea. [4]Interdisciplinary Program for Bioengineering, Seoul National University, Seoul, Republic of Korea. [5]School of Health and Environmental Science, Korea University, Seoul, Republic of Korea. [6]Department of Biomedical Sciences, City University of Hong Kong, Kowloon, Hong Kong. [7]Cell Death Disease Research Center, The Catholic University of Korea, Seoul, Republic of Korea. [8]Institute of Chemical Processes, Seoul National University, Seoul, Republic of Korea. [9]Institute of Engineering Research, Seoul National University, Seoul, Republic of Korea. [10]Bio-MAX Institute, Seoul National University, Seoul, Republic of Korea. [11]These authors contributed equally: Cheesue Kim, Hyeok Kim, Woo-Sup Sim. ✉e-mail: cardioman@catholic.ac.kr; byungskim@snu.ac.kr

instrumental in orchestrating the resolution of inflammation after MI[13–15]. This is because cardiac macrophage efferocytosis of apoptotic neutrophils results in macrophage polarization into pro-reparatory macrophages[16,17]. Overall, the detrimental effects of neutrophils at the early stages of MI pathogenesis outweigh their reparatory effects[4], highlighting the need to downregulate neutrophil-mediated inflammation and promote neutrophil-mediated healing.

Neutrophil targeting has emerged as an attractive therapeutic strategy for MI treatment, given the dynamic roles of neutrophils after MI[7,18,19]. However, several preclinical and clinical studies that employ either small molecules which downregulate neutrophil activation or neutrophil-depleting antibodies, have failed to demonstrate therapeutic efficacy[16,20–22]. This may be because, as demonstrated by a previous study, cardiac neutrophils are necessary for cardiac macrophage efferocytosis and M2 polarization[16]. The dearth of neutrophil-specific moieties owing to their similarity with other myeloid lineage cells also makes it difficult to target neutrophils with high specificity, which increases the risk of off-target effects[22–24]. Clinical trials involving neutrophil downregulation have often shown disappointing efficacy and adverse side effects[20,21].

Here, we show that poly(lactic-co-glycolic acid) (PLGA) nanoparticles can be tuned to offer unique characteristics for neutrophil modulation. PLGA nanoparticles are readily taken up by neutrophils[25–27]. We modified PLGA nanoparticles to release drug in response to ROS produced under inflammatory conditions, which could allow for drug delivery to activated neutrophils at the infarct site. In this study, we fabricated hydrogen peroxide (H_2O_2)-responsive, roscovitine- and catalase-loaded PLGA nanoparticles (RC NPs). RC NPs can be readily taken up by neutrophils migrating to the infarcted heart. Activated neutrophils at the infarcted heart generate H_2O_2 which would be converted to oxygen by the catalase in RC NPs. The buildup of oxygen gas would cause internalized RC NPs to detonate and rapidly release roscovitine in the neutrophils (Fig. 1). Roscovitine is a cyclin-dependent kinase inhibitor that has been shown to effectively induce neutrophil apoptosis and has demonstrated to be safe in clinical trials[28–30]. By loading roscovitine inside RC NPs, activated neutrophils can undergo apoptosis specifically within the infarcted heart, thereby mitigating neutrophil-mediated cardiac damage. RC NP-induced-apoptotic neutrophils can then promote cardiac macrophage efferocytosis and subsequent M2 polarization[17]. Previous strategies which employed small molecules or neutrophil-depleting antibodies to downregulate neutrophil activation, impair M2 polarization[16,20–22]. In contrast, RC NPs could offer a more balanced mode of modulating neutrophils and macrophages, both of which are essential for cardiac repair. We investigated the effect of RC NPs on initial cardiac pathology, cardiac remodeling, and heart function. Here, we demonstrate that a single intravenous injection of RC NPs in MI rats induces robust neutrophil apoptosis at the infarct heart. This leads to subsequent reparatory macrophage polarization and ultimately preserves heart function. This study highlights the therapeutic potential of targeting neutrophils to modulate inflammatory and reparatory processes following MI.

Results

Design and characterization of H_2O_2-responsive RC NPs

Several previous studies have demonstrated neutrophil tropism for nanoparticles[25], particularly for PLGA nanoparticles with sizes ranging between 350 and 500 nm and negative surface charges[26,27,31], and we designed our nanoparticles to fit within this mold. RC NPs had hydrodynamic diameters of 429.7 ± 72.8 nm with a polydispersity index (PDI) of 0.058 and a zeta potential of −25.5 ± 4.9 mV (Fig. 2a). To encapsulate both the water-insoluble drug roscovitine and the water-soluble enzyme catalase, RC NPs were prepared by a two-step water-in-oil-in-water emulsification procedure, resulting in a homogenous capsule-like structure (Fig. 2b). RC NPs displayed stability in both phosphate buffered saline (PBS) and serum conditions over 7 days at 37 °C (Fig. 2c). Catalase loaded in RC NPs reacted with H_2O_2 (Fig. 2d) and produced oxygen (Fig. 2e). RC NPs released roscovitine at a faster rate under H_2O_2 conditions than without H_2O_2 (Fig. 2f). Extracellular H_2O_2 concentration of phorbol-12-myristate-13-acetate (PMA)-activated neutrophils is ~65 μM[32]. Also, extracellular H_2O_2 concentration can reach up to 100 μM after ischemia reperfusion injury[33]. Our nanoparticles act inside neutrophils, and intracellular H_2O_2 concentration is expected to be higher than extracellular H_2O_2 concentration. Therefore, we used H_2O_2 concentrations of greater than 65 μM, specifically, 100 and 200 μM in Fig. 2f. Rapid rather than sustained roscovitine release is crucial for neutrophil targeting as neutrophils are inherently short-lived cells and NETosis, the predominant form of neutrophil death under inflammatory conditions, is hypothesized to take place within 3 to 8 hours after neutrophil activation[34]. We were able to confirm that the elevated rate of drug release under H_2O_2 conditions was due to catalase as R NPs (PLGA nanoparticles with roscovitine but without catalase) under H_2O_2 conditions displayed drug release kinetics similar to that of RC NPs under normal conditions (Fig. 2f). Also, the rates of roscovitine release from R NPs and RC NPs were similar in non-H_2O_2 conditions, which suggests that catalase does not affect drug release in non-H_2O_2 conditions. All NPs displayed over 30% roscovitine release within the first 12 to 24 h (Fig. 2f). The initial burst release of roscovitine in the R NP groups and the non H_2O_2-treated RC NP group can be attributed to a combination of PLGA degradation and drug diffusion, which initiate in the first few days after incubation in water[35–42]. The enhanced rate of drug release in the H_2O_2-treated RC NP groups can be attributed to morphological deformation (Fig. 2g) in addition to PLGA degradation and drug diffusion. RC NPs were found to detonate in response to H_2O_2 with the extent of morphological deformation getting more pronounced as time progressed (Fig. 2g). RC NPs that were not exposed to H_2O_2 and R NPs that were exposed to H_2O_2 did not show any discernable changes.

Next, we tested the cytocompatibility of RC NPs with neutrophils in vitro. Over 90% of neutrophils were RC NP^+ after one hour (Supplementary Fig. 1) and RC NP internalization was verified by confocal microscopy after 2 hours (Fig. 2h). To test whether RC NP internalization could affect the migratory capacity of neutrophils, we conducted a transwell migration assay using formylmethionylleucylphenylalanine (fMLP), a neutrophil chemotactic peptide[43], to create a chemokine gradient between the upper and lower chambers. Neutrophils were observed to migrate through the transwell at a threefold higher rate due to the fMLP gradient (Supplementary Fig. 2) and the number of migrating neutrophils was unchanged upon addition of varying numbers of RC NPs (Fig. 2i). RC NP uptake did not induce aberrant activation or apoptosis of unactivated neutrophils in vitro. RC NP-treated neutrophils showed similar SYTOX Green (a dye that stains strongly for NETs) intensities compared with PBS-treated neutrophils and significantly weaker intensities compared with neutrophils treated with PMA, a protein kinase C activator that induces potent neutrophil activation, ROS generation, and NET formation[44] (Fig. 2j). These data indicate that RC NP uptake did not induce neutrophil activation and NET release. Neutrophils treated with RC NPs containing lethal doses of roscovitine (20 μM) exhibited over 90% viability 6 h after treatment, significantly higher than that of neutrophils treated with equimolar concentrations of roscovitine in its free form (Fig. 2k, Supplementary Fig. 3). This is important as indiscriminate neutrophil killing can (1) reduce the number of neutrophils undergoing apoptosis at the desired injury site, thereby reducing the efferocytosis capacity of cardiac macrophages and (2) increase the risk of adverse effects such as neutropenia. In sum, RC NPs were designed for optimal neutrophil tropism, H_2O_2-responsive roscovitine release, and cytocompatibility.

RC NPs modulate neutrophil fate in vitro

Neutrophils activated in vitro by PMA or in vivo by DAMPs generate ROS (including micromolar concentrations of H_2O_2[32,45]), release

https://doi.org/10.1038/s41467-024-52812-6

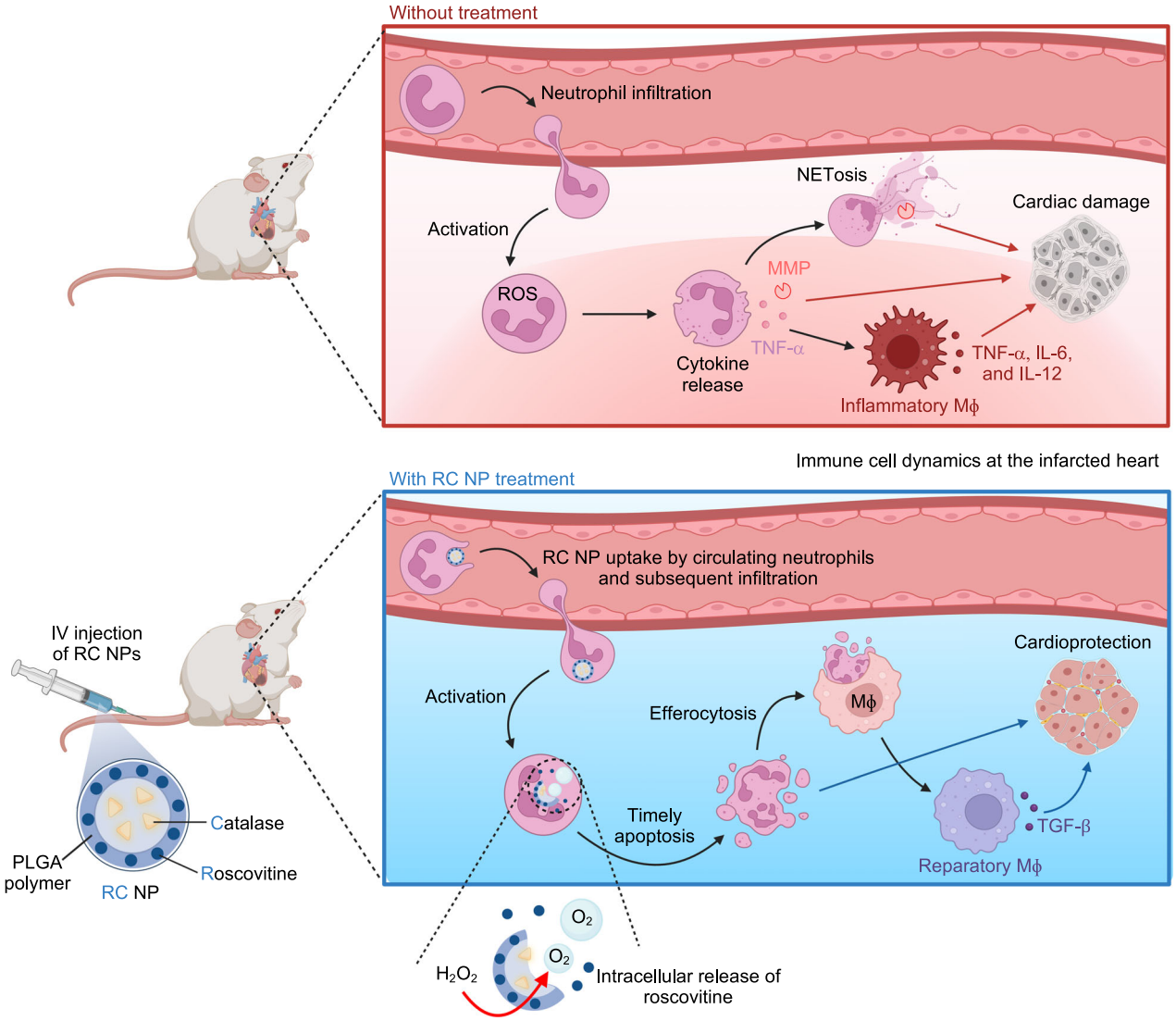

Fig. 1 | Schematic illustration of neutrophil and macrophage (Mϕ) dynamics in the heart following myocardial infarction (MI) with and without intravenous injection of roscovitine/catalase-loaded poly(lactide-co-glycolide) nanoparticles (RC NPs). Neutrophils infiltrate the ischemic heart shortly after MI, where they are activated by stimuli from dying cardiac cells. (Upper panel) Activated neutrophils produce reactive oxygen species (ROS, e.g., H_2O_2) and secrete MMPs, inflammatory cytokines, and NETs that promote cardiomyocyte apoptosis and tissue destruction. Overexuberant neutrophil signaling also suppresses reparatory processes mediated by Mϕs by promoting pro-inflammatory macrophage signaling. These processes collectively impair heart function. (Lower panel) Intravenously injected RC NPs are taken up by neutrophils migrating to the ischemic heart. At the infarct area, H_2O_2 produced by activated neutrophils is converted to oxygen by catalase in RC NPs. The buildup of oxygen gas in RC NPs causes the nanoparticles to explode and rapidly release roscovitine, inducing timely neutrophil apoptosis. This inhibits neutrophil-mediated inflammation and promotes Mϕ polarization to the reparatory phenotype, ultimately protecting the heart from MI damage. Created in BioRender. Kim, B. (2024) BioRender.com/c60t349.

pro-inflammatory cytokines and proteases through ROS-dependent pathways, and finally undergo NETosis. We hypothesized that H_2O_2 produced by activated RC NP$^+$ neutrophils could be consumed by the internalized RC NPs and trigger the release of roscovitine, which would induce timely neutrophil apoptosis to limit secretion of TNF-α, pro-MMP-9, and neutrophil elastase (Fig. 3a). The terminal deoxynucleotidyl transferase dUTP nick end labeling (TUNEL) assay is one of the most reliable methods to measure apoptosis of activated neutrophils as several other viability assays (Annexin V, propidium iodide, 3-(4,5-dimethylthiazol-2-yl)−2,5-diphenyltetrazolium bromide, etc.) are unsuitable in discriminating between NETosis and apoptosis[46]. PMA treatment significantly reduced the fraction of neutrophils undergoing apoptosis (Supplementary Fig. 4). To test whether RC NPs could redirect activated neutrophils to apoptosis, neutrophils were first treated with nanoparticles or their free drug counterparts in vitro and activated with PMA two hours later. We observed that RC NP treatment significantly enhanced the proportion of apoptotic neutrophils compared with PBS treatment in PMA-activated neutrophils (Fig. 3b). This effect was contingent on the elevated rate of roscovitine release from RC NPs as nanoparticles without either catalase or roscovitine (R NPs and C NPs respectively) did not induce significant neutrophil apoptosis. Roscovitine in its soluble form (Free R) and roscovitine and catalase in their soluble forms (Free RC) served as positive controls to verify the immunomodulatory effects of roscovitine on neutrophils. The increase in apoptosis in RC NP-, Free R-, and Free RC-treated PMA-activated neutrophils was inversely proportional to the extent of NETosis (Fig. 3c). While C NPs suppressed NETosis in PMA-activated neutrophils (Fig. 3c), the relative abundance of SYTOX Green-negative nuclei and the low percentage of TUNEL$^+$ cells (Fig. 3b) show that C NPs promote neutrophil survival but are unable to redirect activated neutrophils to apoptosis. These findings are in line with that of previous studies that use exogenous catalase to reduce PMA-induced NETosis and/or extend

https://doi.org/10.1038/s41467-024-52812-6

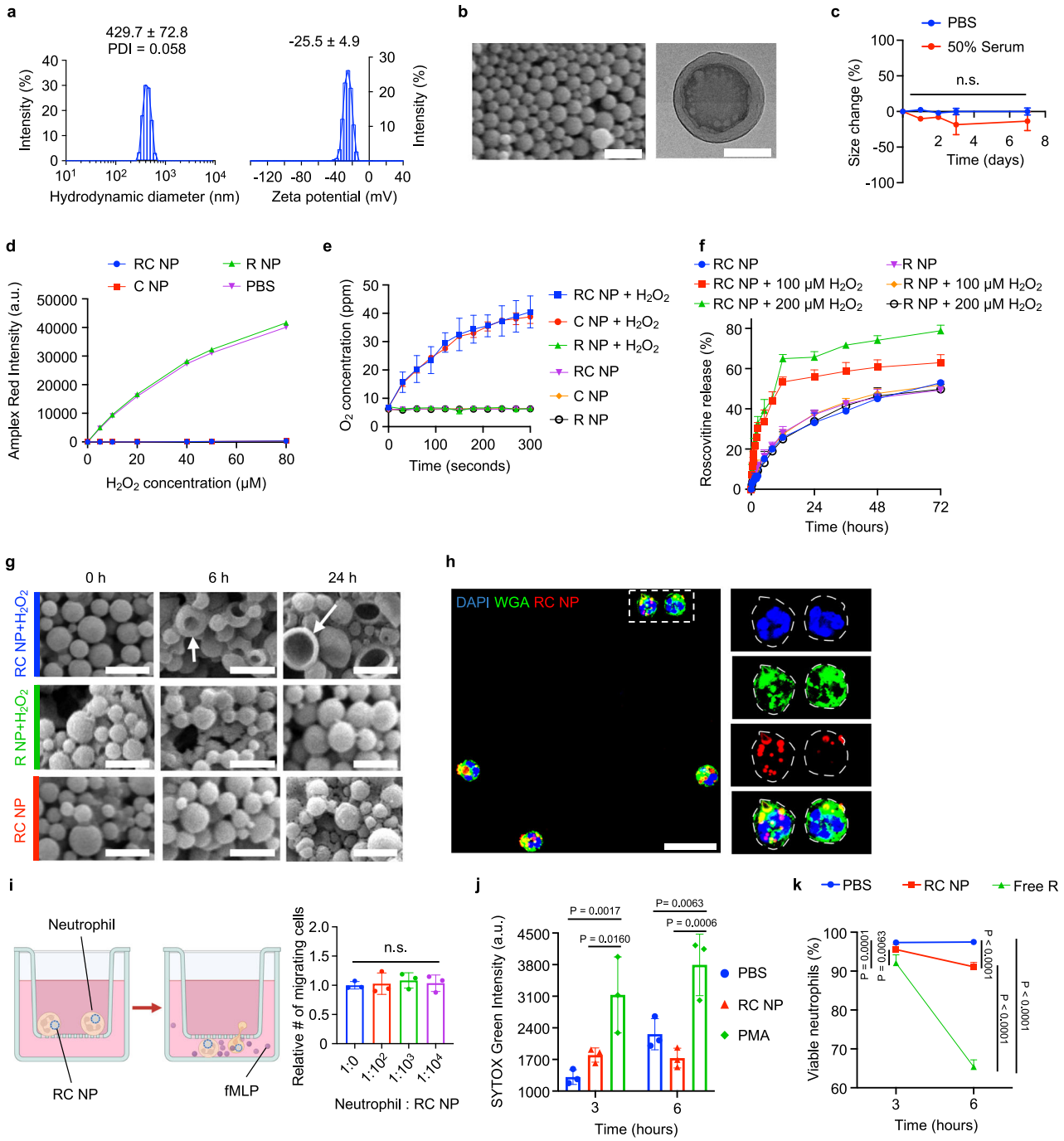

Fig. 2 | Characterization of RC NPs. a Hydrodynamic diameter and zeta potential of RC NPs determined by dynamic and electrophoretic light scattering respectively ($n = 7$). **b** Scanning electron microscopy (SEM, left) and transmission electron microscopy (TEM, right) images of RC NPs. Scale bars, 1 μm (SEM) and 200 nm (TEM). **c** RC NP size stability in PBS and 50% serum at 37 °C ($n = 3$ biological replicates; n.s., not significant). **d** Remaining amount (Amplex Red intensity) of H_2O_2 after reaction with nanoparticles at various H_2O_2 concentrations ($n = 3$ biological replicates). **e** Oxygen production by RC NPs under H_2O_2 conditions ($n = 3$ biological replicates). **f** Accelerated roscovitine release from RC NPs under H_2O_2 conditions ($n = 3$ biological replicates). **g** Time-dependent deformation (arrows) of RC NPs upon addition of H_2O_2 determined by SEM. Scale bars, 1 μm. **h** RC NP uptake by neutrophils visualized by confocal microscopy. Scale bar, 20 μm. WGA stains for cell membrane. Dotted lines show edge of cell membrane. **i** Effect of RC NPs on neutrophil migration along chemokine (fMLP, 1 μM) gradient ($n = 3$ biological replicates; n.s., not significant). **j** SYTOX Green intensity of neutrophils following treatment with various agents ($n = 3$ biological replicates). PMA (100 nM) served as a positive control. **k** Neutrophil viability following treatment with various agents ($n = 4$ biological replicates). Free roscovitine (R; 20 μM) served as a positive control. All data presented as mean ± standard deviation (SD). One-way ANOVA was used for the comparison in **i**. Two-way ANOVA was used for the comparisons in **c**, **j**, **k**. Experiments in **b**, **g**, **h** were each performed thrice independently, yielding similar results each time. Schematic in **i** created in BioRender. Kim, B. (2024) BioRender.com/c05i014.

neutrophil lifespan in vitro[46,47]. Extended neutrophil survival however had little to no effect on the secretion of proteases and cytokines by PMA-activated neutrophils. Activated neutrophils that were redirected by RC NPs, Free R, or Free RC to apoptosis secreted significantly lower levels of TNF-α, pro-MMP-9, and elastase than PBS-, R NP-, and C NP-treated neutrophils (Fig. 3d–f). RC NPs therefore induce timely apoptosis in activated neutrophils, reducing NETosis and the secretion of pro-inflammatory cytokines and proteases.

https://doi.org/10.1038/s41467-024-52812-6

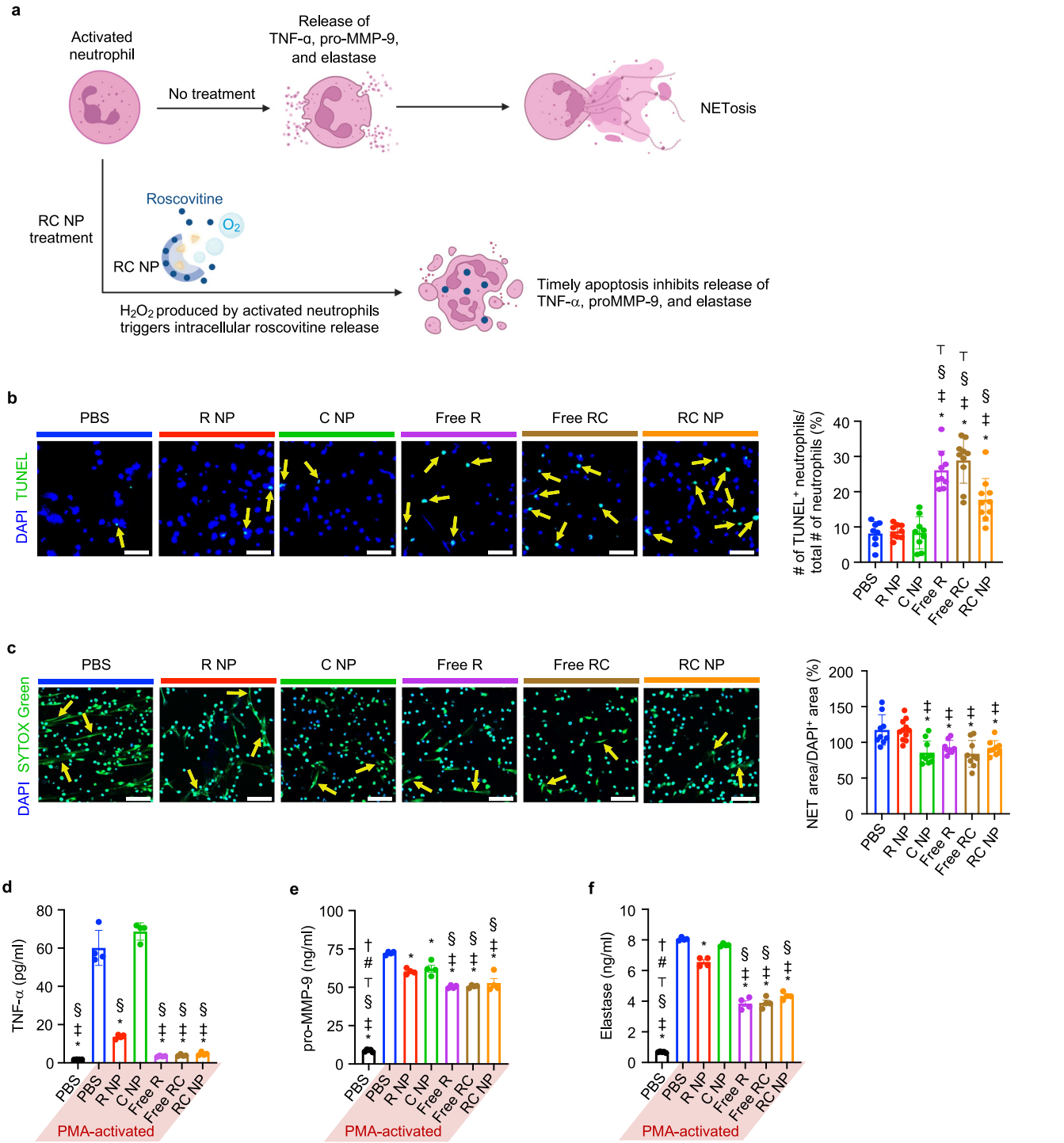

Fig. 3 | RC NP-mediated modulation of neutrophil fate in vitro. a Diagram illustrating RC NP modulation of activated neutrophils. **b** RC NP (50 μM) treatment induces apoptosis (arrows) of PMA (750 nM)-activated neutrophils as determined by the TUNEL assay (biological replicates $n = 8$ for PBS, 9 for R NP, C NP, and Free R, and 10 for Free RC and RC NP). Scale bars, 50 μm. **c** RC NP intervention reduces the amount of NETs (arrows) extruded from PMA-activated neutrophils as determined by SYTOX Green staining (biological replicates $n = 8$ for Free R, 9 for PBS, Free RC, and RC NP, 10 for C NP, and 11 for R NP). Scale bars, 50 μm. RC NP-induced apoptosis of activated neutrophils decreases secretion of **d** TNF-α ($n = 4$ biological replicates), **e** pro-MMP-9 (biological replicates $n = 4$ for all PMA-activated groups, 5 for PBS), and **f** elastase as determined by enzyme-linked immunosorbent assays (ELISAs) (biological replicates $n = 4$ for all PMA-activated groups, 5 for PBS). $^{*}p < 0.05$ versus PBS (PMA-activated); $^{‡}p < 0.05$ vs R NP; $^{§}p < 0.05$ vs C NP; $^{⊤}p < 0.05$ versus RC NP; $^{\#}p < 0.05$ vs Free R; $^{†}p < 0.05$ vs Free RC. All data presented as mean ± SD. One-way ANOVA was used for all comparisons. Figure **a** created in BioRender. Kim, B. (2024) BioRender.com/h86n476.

Apoptotic neutrophils promote macrophage polarization

Neutrophils at the ischemic site are critical in mediating the resolution of inflammation by promoting the development of reparatory macrophages. One way in which neutrophils promote macrophage polarization is through their apoptosis[14]. Apoptotic neutrophils allow for myeloid-epithelial-reproductive tyrosine kinase (MertK)-mediated macrophage efferocytosis, and activate an anti-inflammatory response in macrophages characterized by reduced secretion of pro-inflammatory cytokines and increased secretion of TGF-β1[16]. To investigate the impact of RC NP-treated PMA-activated neutrophils on

https://doi.org/10.1038/s41467-024-52812-6

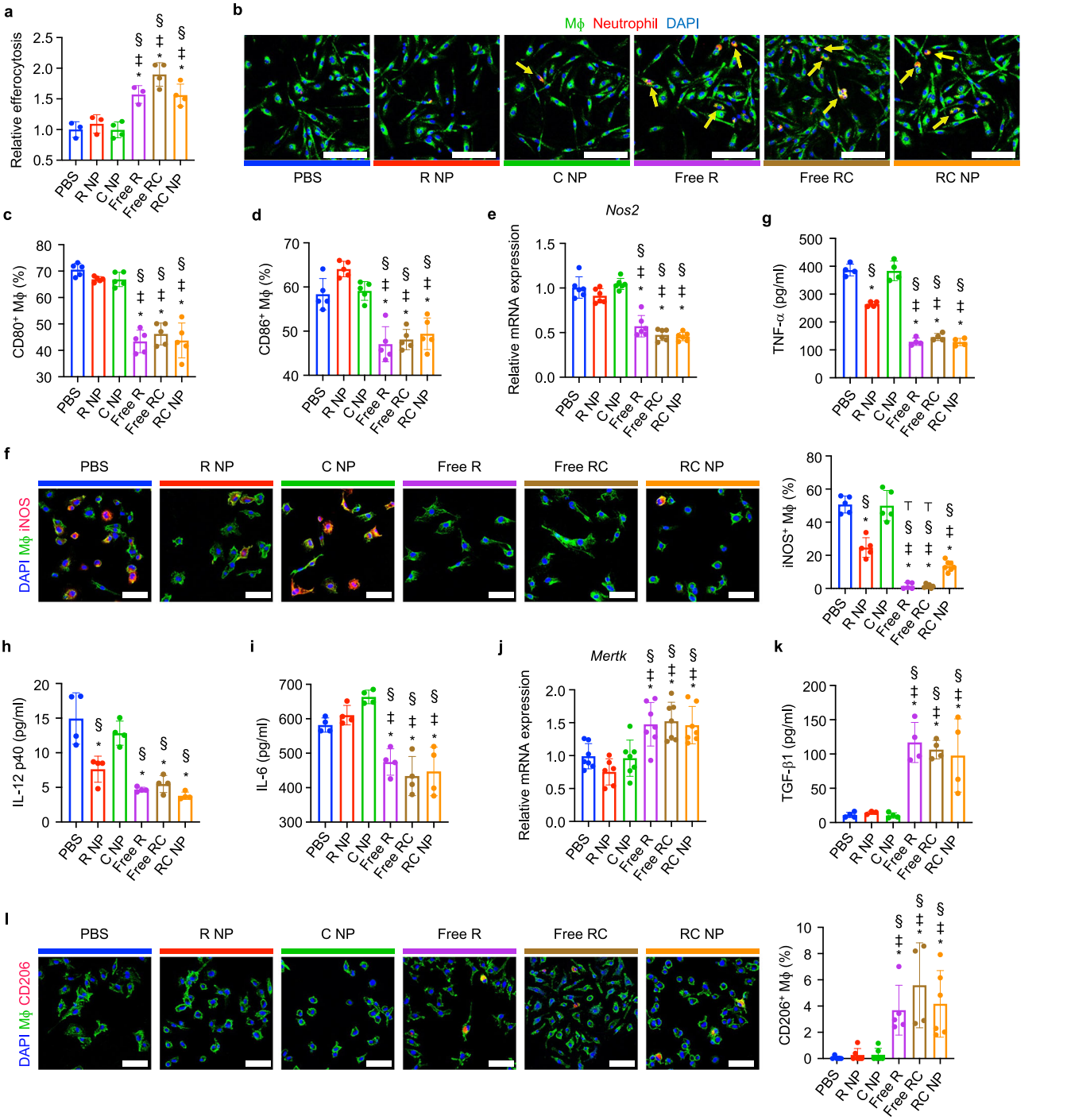

Fig. 4 | Macrophage efferocytosis and polarization by RC NP⁺ apoptotic neutrophils. RC NP treatment of PMA-activated neutrophils enhances their efferocytosis (arrows) by LPS (1 ng/ml)-treated Mϕs as verified by **a** flow cytometry (20 min after coculture) and **b** confocal microscopy (40 min after coculture) (biological replicates $n = 3$ for PBS, R NP, and Free R, and 4 for C NP, Free RC, and RC NP). Scale bars, 100 μm. Relative efferocytosis was calculated by analyzing the percentage of F4/80⁺ macrophages positive for DiD due to efferocytosis of DiD-labeled neutrophils and normalized to the PBS group. Flow cytometric analysis of **c** CD80 and **d** CD86 expression by F4/80⁺ Mϕs ($n = 5$ biological replicates). **e** Relative mRNA expression of *Nos2* as determined by PCR ($n = 6$ biological replicates). **f** Representative immunofluorescence images and quantitative analysis of iNOS expression (biological replicates $n = 5$ for PBS, R NP, C NP, and Free R, 6 for Free RC, and 7 for RC NP). Scale bars, 50 μm. Secretion of **g** TNF-α, **h** IL-12 p40, and **i** IL-6 as determined by ELISA ($n = 4$ biological replicates). **j** Relative mRNA expression of *Mertk* as determined by PCR (biological replicates $n = 6$ for R NP, 7 for all other groups). **k** Secretion of TGF-β1 as determined by ELISA (biological replicates $n = 3$ for R NP, 4 for all other groups). **l** Representative immunofluorescence images and quantitative analysis of CD206 expression (biological replicates $n = 4$ for Free RC, 5 for PBS and Free R, and 6 for all other groups). Scale bars, 50 μm. $^{*}p < 0.05$ vs PBS; $^{‡}p < 0.05$ vs R NP; $^{§}p < 0.05$ vs C NP; $^{⊤}p < 0.05$ vs RC NP. All data presented as mean ± SD. One-way ANOVA was used for all comparisons.

https://doi.org/10.1038/s41467-024-52812-6

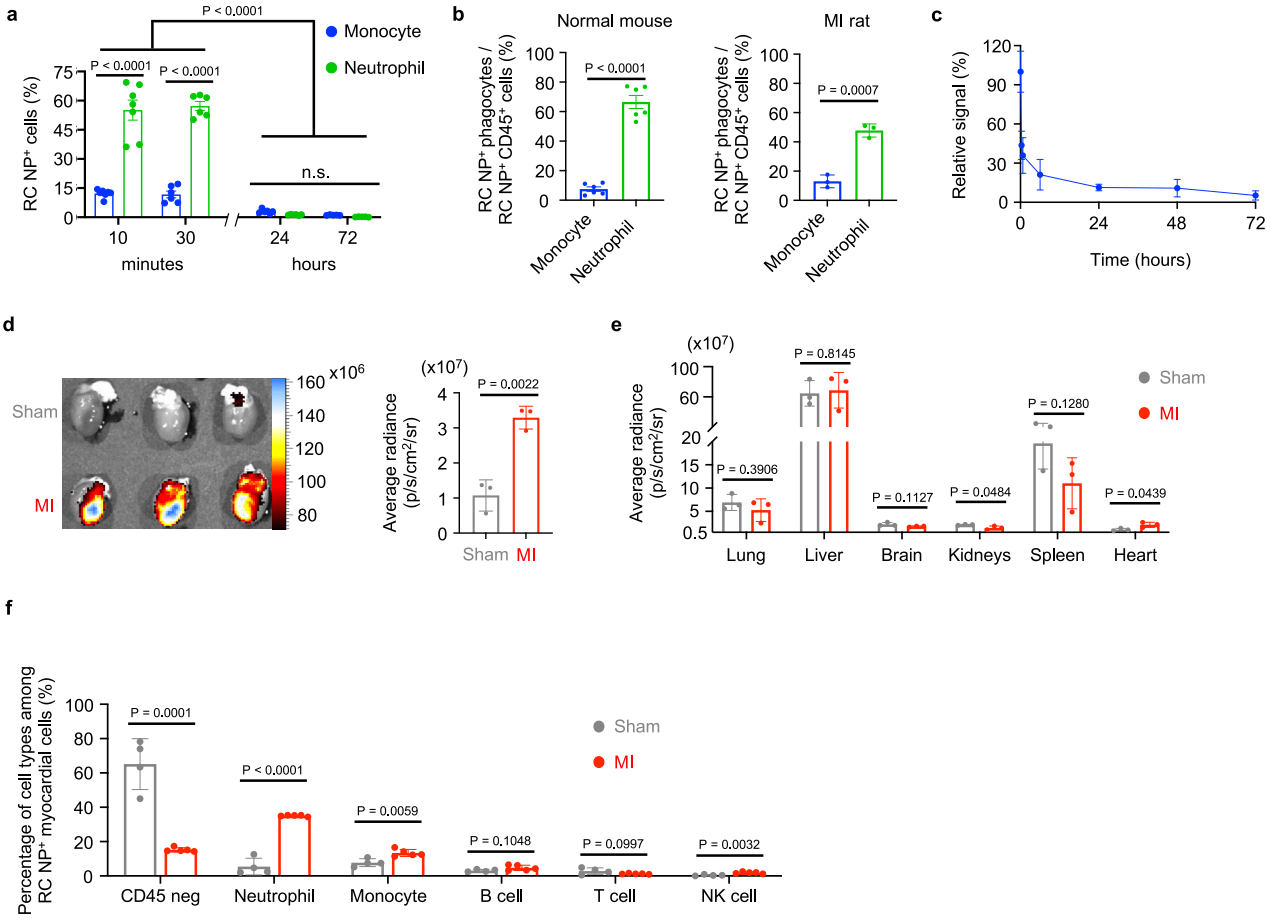

Fig. 5 | Biodistribution of RC NPs. a RC NP uptake by circulating monocytes and neutrophils at various time points after intravenous injection in uninjured mice as assessed by flow cytometry ($n = 5$ mice for 72 h, $n = 6$ mice for 30 min and 24 h, and 7 mice for 10 min). **b** Percentage of RC NP$^+$CD45$^+$ monocytes and neutrophils among all circulating RC NP$^+$CD45$^+$ cells 30 min after intravenous injection in both uninjured mice and MI rats as determined by flow cytometry ($n = 3$ MI rats and 6 normal mice). **c** Pharmacokinetics of DiR-labeled RC NPs in the bloodstream following intravenous injection in uninjured rats ($n = 3$). **d** Ex vivo images and average radiance of sham and MI hearts 24 h after intravenous injection of DiD-labeled RC NPs ($n = 3$). **e** Average radiance of DiD-labeled RC NPs in major organs of sham and MI rats ($n = 3$; n.s., not significant). **f** Flow cytometric analysis to determine the various cell types responsible for RC NP uptake in sham and MI hearts 24 h after intravenous injection of DiD-labeled RC NPs ($n = 4$ for sham, 5 for MI). All data presented as mean ± SD. Two-way ANOVA was used for the comparisons in **a** (Sidak when comparing between cells, Tukey when comparing between time points). Multiple unpaired two-sample *t* tests were used for the comparisons in **f**. Unpaired two-sided *t* tests were used for comparisons in **b**–**e**.

macrophages, we conducted an in vitro coculture assay. Neutrophils treated with nanoparticles or corresponding free drugs were activated with PMA and then fed to macrophages together with lipopolysaccharide (LPS), which served to mimic the inflammatory MI microenvironment. Flow cytometry (Fig. 4a) and confocal imaging (Fig. 4b) showed that macrophage efferocytosis of RC NP-treated PMA-activated neutrophils was significantly higher than that of PBS-, C NP-, or R NP-treated PMA-activated neutrophils. Enhanced efferocytosis of apoptotic neutrophils by macrophages promoted the development of a pro-reparatory phenotype as determined by flow cytometry, quantitative reverse transcription-polymerase chain reaction (qRT-PCR), enzyme-linked immunosorbent assay (ELISA), and immunocytochemistry (ICC). Significantly fewer macrophages cultured with either RC NP-, Free R-, or Free RC-treated PMA-activated neutrophils displayed the costimulatory B7 molecules CD80 and CD86 compared with macrophages cultured with either PBS-, R NP-, or C NP-treated PMA-activated neutrophils (Fig. 4c, d, and Supplementary Fig. 5). Similarly, mRNA and protein expressions of inducible nitric oxide synthase (*Nos2* and iNOS respectively) (Fig. 4e, f) and secretion of pro-inflammatory cytokines TNF-α (Fig. 4g), IL-12 p40 subunit (Fig. 4h), and IL-6 (Fig. 4i) were significantly lower in macrophages cultured with RC NP-treated PMA-activated neutrophils compared with macrophages cultured with PBS-treated PMA-activated neutrophils. mRNA expression of *Mertk* (Fig. 4j), secretion of pro-resolving cytokine TGF-β1 (Fig. 4k), and protein expression of CD206 (Fig. 4l) were also significantly higher in RC NP-, Free R- and Free RC-treated groups compared with other groups. Taken together, RC NPs can indirectly promote the development of pro-reparatory macrophages by enhancing neutrophil apoptosis and subsequent macrophage efferocytosis.

Biodistribution of RC NPs in vivo

Nanoparticle uptake by circulating cells in vivo can mainly be attributed to monocytes and neutrophils[48]. We intravenously injected RC NPs into BALB/c mice and analyzed the fraction of circulating RC NP$^+$ monocytes and neutrophils at various time points after injection. BALB/c mice were our model organism of choice for determining relative nanoparticle uptake by circulating phagocytes as both neutrophils and monocytes are well-defined in mice compared with rats and other animals. The percentage of RC NP uptake in CD45$^+$Ly6G + CD11b$^+$ neutrophils exceeded 55% 10 and 30 min after injection and was consistently higher in neutrophils than in CD45$^+$Ly6G$^-$CD11b$^+$Ly6C$^+$ monocytes at these early time points (Fig. 5a, Supplementary Fig. 6a). Thirty minutes after injection, over 47% of circulating RC NP$^+$ cells were neutrophils in both normal mice and MI

Fischer 344 (F344) rats while less than 14% were monocytes (Fig. 5b, Supplementary Figs. 6b, 7). Collectively, our data show high neutrophil tropism and selectivity for RC NPs at early time points after RC NP injection. However, we noticed that the percentage of circulating RC NP$^+$ neutrophils and monocytes decreased significantly after 24 and 72 h (Fig. 5a). This can be attributed to the short circulating half-lives of neutrophils and monocytes[49,50]. Our pharmacokinetic data show that RC NPs also have a short half-life in vivo (Fig. 5c). We observed a sharp decrease in the fluorescence signal of DiR-labeled RC NPs within 24 h of intravenous injection followed by a sustained decrease in fluorescence signal up to 72 h after injection. RC NPs were then intravenously injected into sham and MI F344 rats and found to accumulate at a 3.0-fold higher level in the hearts of MI rats than in the hearts of sham rats (Fig. 5d). A high portion of the injected RC NPs also accumulated in the livers, spleens, and lungs of sham and MI rats (Fig. 5e). Importantly, the average radiance of MI hearts was significantly higher than that of sham hearts (Fig. 5e). F344 rats were our model organism of choice for MI experiments as the MI rat model exhibits smaller variance, allows for more precise image acquisition, and more closely mimics human pathology compared with mouse models[51]. Flow cytometry analysis revealed that the composition of RC NP$^+$ cells was significantly different between MI and sham rats (Fig. 5f, Supplementary Fig. 8). 15.2% of all RC NP$^+$ cells in the hearts of MI rats were CD45 negative cells while 65.2% of all RC NP$^+$ cells in the hearts of sham rats were CD45 negative cells (Fig. 5f, Supplementary Fig. 8). 35.1% of all RC NP$^+$ cells in the hearts of MI rats were neutrophils while only 5.4% of all RC NP$^+$ cells in the hearts of sham rats were neutrophils. 13.4% of all RC NP$^+$ cells in the hearts of MI rats were monocytes, while 7.7% of all RC NP$^+$ cells in the hearts of sham rats were monocytes. Other immune cell types such as B cells, T cells, and NK cells each made up 5% or less of all the RC NP$^+$ cells in the hearts of both MI and sham rats.

RC NPs modulate immune cell dynamics post-MI

RC NPs were intravenously injected into F344 rats one hour after MI and cardiac neutrophils and macrophages were analyzed 24 and 72 h later. The Free RC group was excluded from in vivo analyses due to the poor cellular uptake of catalase in its "free form"[52,53], its rapid degradation by plasma proteases[54,55], and the nonspecific biodistribution and lack of targeting ability of intravenously injected enzymes[56]. Furthermore, there were no significant differences between Free R and Free RC groups in vitro (Figs. 3 and 4), which suggests that there is no added benefit to using catalase in its free form. We found that RC NP injection significantly increased the percentage of TUNEL$^+$ neutrophils in the infarcted heart 24 h after MI (Fig. 6a). This increase in TUNEL$^+$ neutrophils corresponded with a decrease in CitH3$^+$ (a NET marker) neutrophils (Fig. 6b), indicating that RC NPs redirected neutrophils from NETosis to apoptosis. RC NP-mediated neutrophil apoptosis also resulted in a decrease in the percentage of iNOS$^+$ macrophages and an increase in the percentages of CD206$^+$ and Arginase 1$^+$ (Arg1$^+$) macrophages compared with all other groups (Fig. 6c, d, and Supplementary Fig. 9). Flow cytometric analysis of cardiac macrophages also showed that RC NP treatment led to a significant decrease in expression of M1 markers CD86 and CD80 in cardiac macrophages (CD68$^+$ cells) (Fig. 6e, Supplementary Fig. 10). Five days after MI, the numbers of M1 (CD80+) macrophages and neutrophils were significantly decreased in the hearts of RC NP-treated rats compared with that of PBS-treated rats (Supplementary Fig. 11a, b), while the numbers of total leukocytes, macrophages, and T cells in the hearts of MI rats were unchanged by RC NP treatment (Supplementary Fig. 11c–e). These data further reinforce our hypothesis that RC NPs exert their therapeutic effects by modulating cardiac neutrophils and the phenotype of cardiac macrophages. We also observed lower serum levels of NET-associated protein S100A9 and neutrophil granule-derived LL-37 in RC NP-treated MI rats compared with PBS-treated MI rats (Fig. 6f, g). Together, our results indicate that a single injection of RC NPs enables powerful control over neutrophil activation and death in the infarcted heart which subsequently promotes the development of a reparatory macrophage microenvironment.

RC NPs preserve heart function post-MI

MI induction, RC NP injection, Evan's blue (EB) and triphenyltetrazolium (TTC) staining, Masson's trichrome staining, and IHC analysis of myocardium and vessels at border and infarct zones were performed according to the scheme illustrated in Fig. 7a. EB and TTC staining of infarcted hearts 24 h after MI showed similar areas at risk (AAR) among various groups but significantly decreased infarct sizes in Free R- and RC NP-treated rats (Supplementary Fig. 12). Masson's trichrome staining revealed that RC NP treatment significantly reduced the fibrotic scar tissue area while preserving the myocardium (Fig. 7b). TUNEL analysis of infarcted tissues 72 h post-MI showed that RC NP-mediated neutrophil modulation significantly protected cardiomyocytes and cardiac endothelial cells from neutrophil-mediated cell death (Fig. 7c,d). Improved cardiomyocyte and endothelial cell survival at the early stages of MI upon RC NP treatment resulted in a significantly greater cTnT$^+$ myocardium area and CD31$^+$ endothelial cell vessel density at both border and infarct zones 4 weeks post-MI (Fig. 7e, f). The RC NP-mediated decrease in fibrosis and increases in cardiomyocyte and endothelial cell survival in the infarcted heart post-MI collectively resulted in preserved heart function, which was determined using transthoracic echocardiography and pressure-volume (PV) loops according to the scheme shown in Fig. 8a. Echocardiography was conducted 4 h, 3 days, and up to 4 weeks post-MI (Fig. 8b). Ejection fraction and fractional shortening, representative indicators of the left ventricle's (LV) ability to pump out blood, sharply drop after MI and progressively decrease with time. RC NP treatment significantly preserved ejection fraction and fractional shortening post-MI compared with all other treatments (Fig. 8c, d) as soon as 1 week post-MI. Left ventricular internal diameter end diastole (LVIDd) and left ventricular internal diameter end systole (LVIDs), parameters of adverse cardiac remodeling, and anterior wall thickness, a measure of myocardium thickening in the infarct area, were significantly preserved upon RC NP treatment (Fig. 8e–g). In addition, RC NP-treated MI rats showed a significant preservation of global circumferential strain, an index of LV function, 1 and 4 weeks post-MI compared with PBS-treated MI rats (Supplementary Fig. 13). Load independent evaluation of hemodynamic parameters using an invasive PV catheter 4 weeks post-MI showed similarly promising results (Fig. 8h). RC NP-treated MI rats showed significantly higher cardiac output and stroke volume (indicators of the volume of blood pumped from the LV per minute and per beat respectively) (Fig. 8i, j), steeper slopes of end-systolic pressure-volume relationship (ESPVR, a measure of end-systolic ventricular inotropy) and end-diastolic pressure-volume relationship (EDPVR, a measure of end-diastolic ventricular compliance) (Fig. 8k, l), higher maximum and minimum rates of pressure change (dP/dt_{max} and dP/dt_{min}, indicators of myocardial contraction and relaxation respectively) (Fig. 8m, n), and significantly lower maximum volume (V_{max}, a measure of cardiac remodeling at maximum diastole) (Fig. 8o) compared with all other groups. Collectively, our results suggest that RC NP treatment reduces initial cardiac impairment post-MI by protecting cardiomyocytes and cardiac endothelial cells from neutrophil-mediated apoptosis. These effects persist post-MI, preserving and even ameliorating various parameters of heart function. This may be in part due to the reparatory microenvironment generated by cardiac macrophages that have phagocytosed apoptotic, RC NP$^+$ neutrophils. While Free R treatment also resulted in considerable therapeutic benefit compared with PBS treatment in terms of reduced fibrosis, increased myocardium area and endothelial vessel density, improved ejection

https://doi.org/10.1038/s41467-024-52812-6

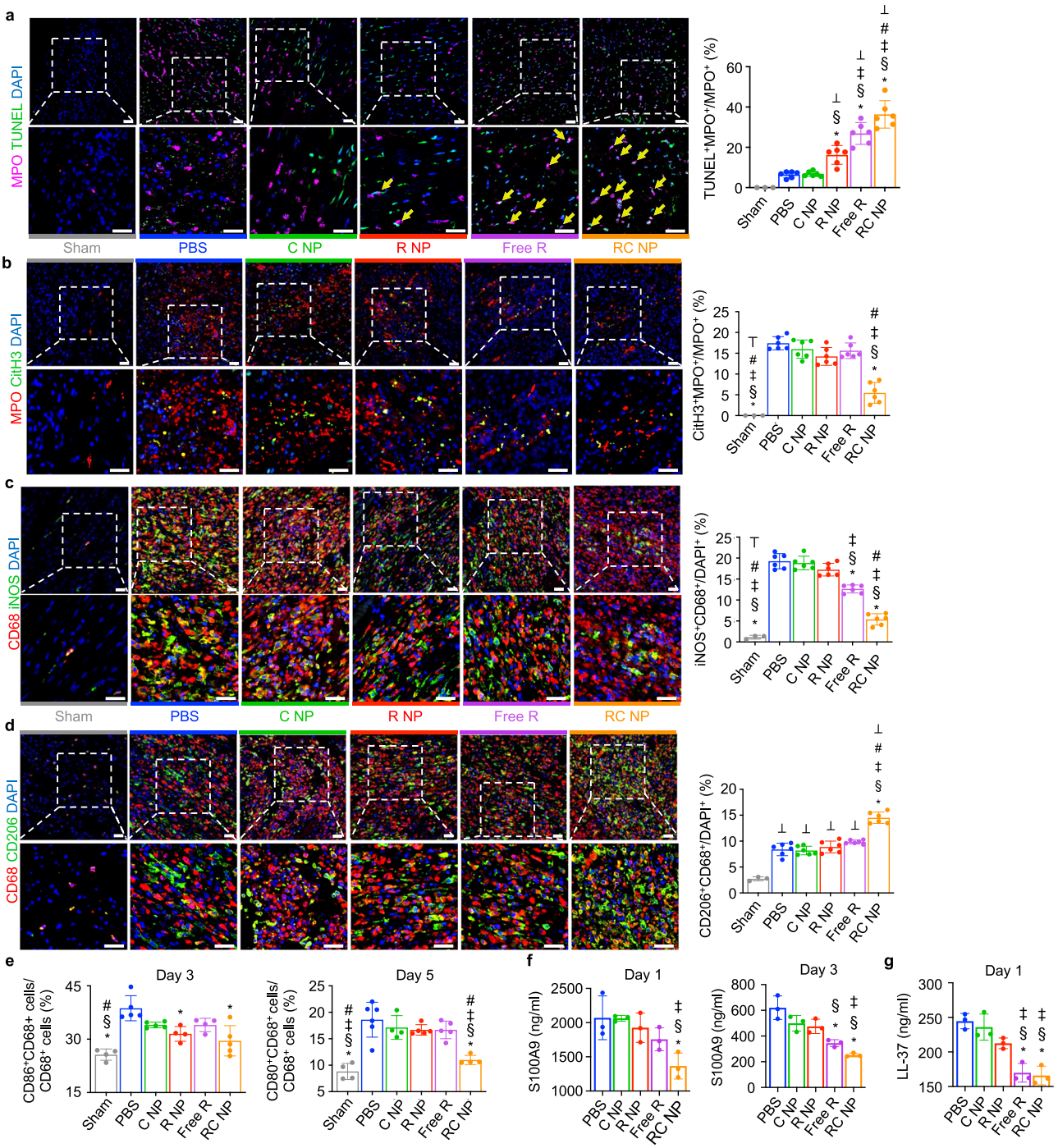

Fig. 6 | RC NP-mediated modulation of immune cell dynamics post-MI. **a** Representative IHC images and quantitative analysis of apoptotic (TUNEL$^+$, green) neutrophils (MPO$^+$, pink) in infarcted rat hearts 1 day post-MI ($n = 3$ for sham, 6 for other groups). Scale bars, 25 μm. **b** Representative IHC images and quantitative analysis of neutrophils (MPO$^+$, red) that have undergone NETosis (CitH3$^+$, green) in infarcted rat hearts 3 days post-MI ($n = 3$ for sham, 6 for other groups). Scale bars, 25 μm. **c** Representative IHC images and quantitative analysis of iNOS$^+$ (green) macrophages (CD68$^+$, red) in infarcted hearts 3 days post-MI ($n = 3$ for sham, 6 for other groups). Scale bars, 25 μm. **d** Representative IHC images and quantitative analysis of CD206$^+$ (green) macrophages (CD68$^+$, red) in infarcted hearts 3 days post-MI ($n = 3$ for sham, 6 for other groups). Scale bars, 25 μm. **e** CD86 and CD80 expression in macrophages (CD68$^+$ cells) 3 and 5 days after MI as determined by flow cytometry (biological replicates $n = 4$ for D3/D5 sham, D3 R NP, D3 Free R, D5 C NP, and D5 RC NP, 5 for D3 PBS, D3 C NP, D3 RC NP, D5 R NP, and D5 Free R, and 6 for D5 PBS). **f** Serum levels of NET-associated chemoattractant protein S100A9 1 and 3 days post-MI as determined by ELISA ($n = 3$ biological replicates). **g** Serum levels of neutrophil granule-derived LL-37 1 day post-MI as determined by ELISA ($n = 3$ biological replicates). *$p < 0.05$ vs PBS; $^{\S}p < 0.05$ vs C NP; $^{\ddagger}p < 0.05$ vs R NP; $^{\#}p < 0.05$ vs Free R; $^{\top}p < 0.05$ vs RC NP; $^{\perp}p < 0.05$ vs Sham. All data presented as mean ± SD. One-way ANOVA was used for all comparisons.

fraction, and other parameters of heart function, RC NPs exhibited significantly higher therapeutic efficacy than the free roscovitine treatment group in most of the aforementioned parameters. We attribute the superior therapeutic efficacy of RC NPs to their ability to preferentially induce apoptosis in activated neutrophils within the infarcted heart, which then promotes macrophage reprogramming (Fig. 6), while Free R indiscriminately affects circulating and cardiac neutrophils, thereby only dampening inflammation in the early

https://doi.org/10.1038/s41467-024-52812-6

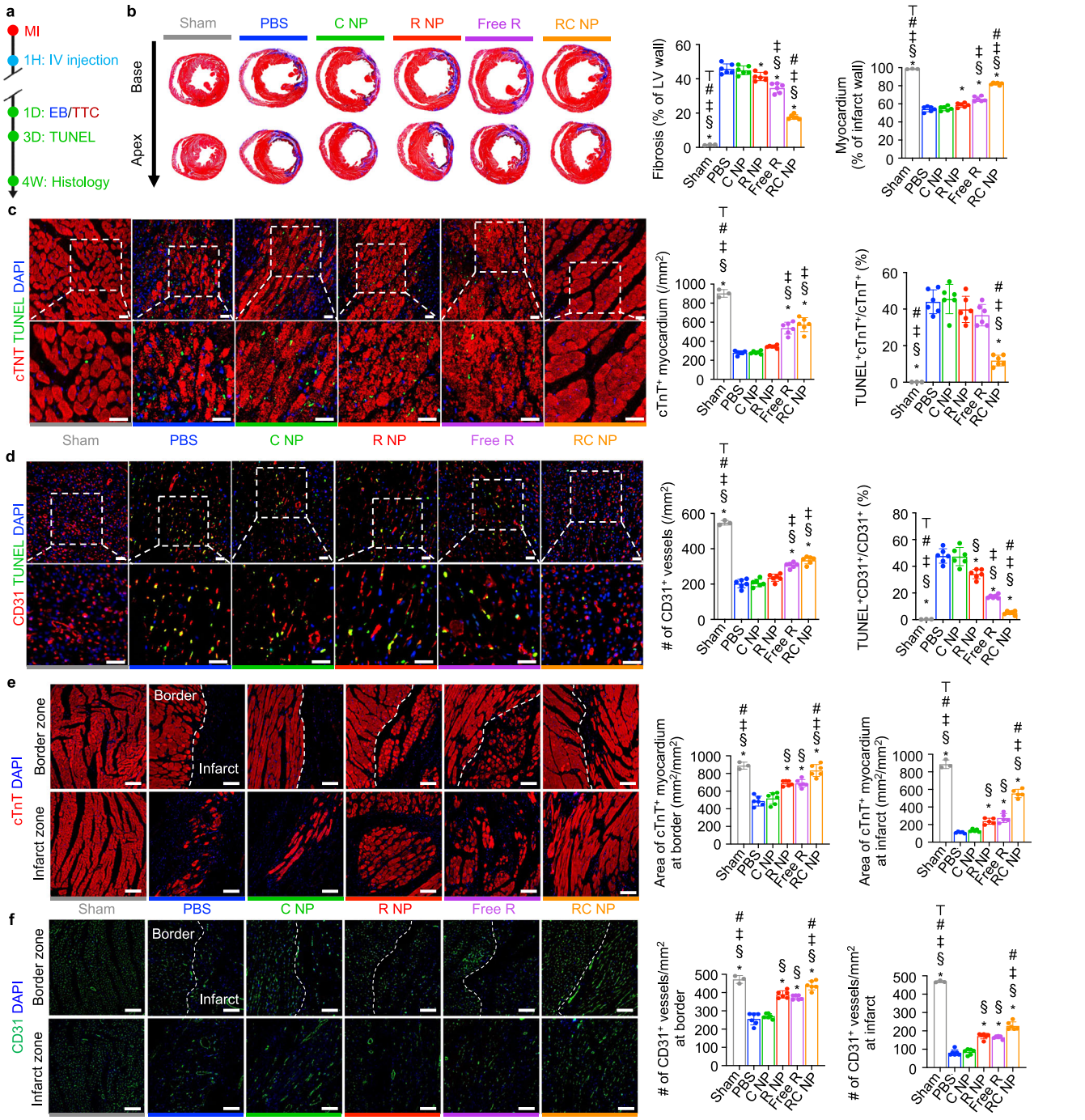

Fig. 7 | RC NPs mitigate adverse remodeling post-MI. a Experimental timeline for in vivo histological analysis of RC NP efficacy. **b** Representative Masson's trichrome-stained histological images of infarcted hearts (purple, scar tissue; red, viable myocardium) and quantification of fibrosis and myocardium 4 weeks after MI ($n = 3$ for sham, 6 for other groups). **c** Representative IHC images and quantitative analysis of cardiomyocytes ($cTnT^+$, red) and apoptotic cardiomyocytes ($TUNEL^+cTnT^+$) at the infarct zone 3 days post-MI ($n = 3$ for sham, 6 for other groups). Scale bars, 25 μm. **d** Representative IHC images and quantitative analysis of endothelial cells ($CD31^+$, red) and apoptotic endothelial cells ($TUNEL^+CD31^+$) at the infarct zone 3 days post-MI ($n = 3$ for sham, 6 for other groups). Scale bars, 25 μm. **e** Representative IHC images and quantitative analysis of cardiomyocytes (cTnT, red) at the border and infarct zones 4 weeks post-MI ($n = 3$ for sham, 6 for other groups). Scale bars, 100 μm. **f** Representative IHC images and quantitative analysis of capillary density (CD31, green) at the border and infarct zones 4 weeks post-MI ($n = 3$ for sham, 6 for other groups). Scale bars, 100 μm. $^*p < 0.05$ vs PBS; $^§p < 0.05$ vs C NP; $^‡p < 0.05$ vs R NP; $^#p < 0.05$ vs Free R; $^⊤p < 0.05$ vs RC NP. All data presented as mean ± SD. One-way ANOVA was used for all comparisons.

stages of MI. This further highlights the potential of targeted, spatiotemporal drug delivery.

Polymorphonucleocyte depletion reduces efficacy of RC NPs

To verify the extent to which the therapeutic effects of RC NPs observed in MI rats could be attributed to neutrophil modulation, we conducted a neutrophil depletion experiment according to the scheme illustrated in Fig. 9a. For our depletion experiments, we used an anti-polymorphonucleocyte (anti-PMN) antiserum that is commonly used to deplete neutrophils in rats[57–59]. Rats not receiving antiserum were injected with equal volumes of control serum. Heart function was determined using transthoracic echocardiography conducted at various

https://doi.org/10.1038/s41467-024-52812-6

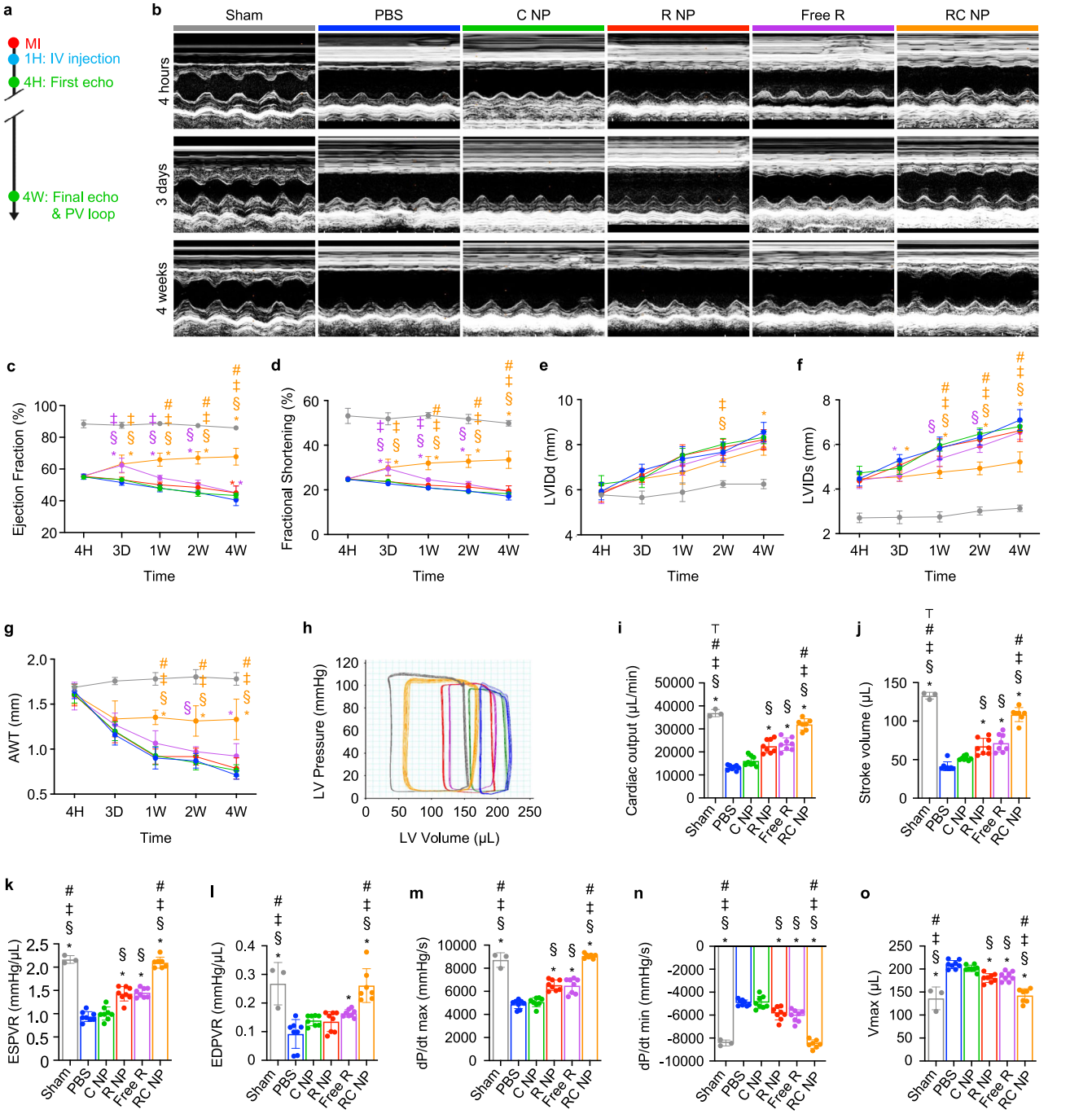

Fig. 8 | RC NP-mediated preservation of heart function post-MI. a Experimental timeline for in vivo analysis of RC NP efficacy. **b** Representative M-mode images at various time points post-MI. **c** Left ventricular ejection fraction, (**d**) fractional shortening, (**e**) LVIDd, (**f**) LVIDs, and (**g**) AWT of MI rats at indicated time points $n = 3$ for sham, 7 for PBS, Free R, and RC NP, 8 for C NP, and 9 for R NP. **h** Representative hemodynamic pressure and volume (PV) curves 4 weeks post-MI. **i** Cardiac output, (**j**) stroke volume, (**k**) ESPVR, (**l**) EDPVR, (**m**) maximal rate of pressure change during systole (dP/dt_{max}), (**n**) minimal rate of pressure change during diastole (dP/dt_{min}), and (**o**) maximum volume (V_{max}) 4 weeks after MI. $n = 3$ for sham, 7 for PBS, Free R, and RC NP, 8 for C NP, and 9 for R NP. $^{*}p < 0.05$ vs PBS; $^{§}p < 0.05$ vs C NP; $^{‡}p < 0.05$ vs R NP; $^{\#}p < 0.05$ vs Free R; $^{⊤}p < 0.05$ vs RC NP. All data presented as mean ± SD. Two-way ANOVA was used for comparisons in **c**–**g**. One-way ANOVA was used for comparisons in **i**–**o**.

time points post-MI (Fig. 9b). Importantly, we found that the ejection fraction and fractional shortening of RC NP-treated rats were significantly higher than those of neutrophil-depleted RC NP-treated rats (Fig. 9c, d). The LVIDs of RC NP-treated rats and neutrophil-depleted RC NP-treated rats were not significantly different (Fig. 9e). However, the LVIDs of RC NP-treated rats were significantly lower than that of PBS-treated rats for 4 weeks post-MI, while the LVIDs of neutrophil-depleted RC NP-treated rats was only significantly lower than that of PBS-treated rats up to 1 week post-MI (Fig. 9e). This slight, transient improvement in LVIDs observed in neutrophil-depleted RC NP-treated MI rats may be due to other cardiac cells, such as macrophages, being affected by the roscovitine released by RC NPs[60,61]. The LVIDd of RC NP-treated rats and neutrophil-depleted RC NP-treated rats showed no significant difference (Fig. 9f). Collectively, our neutrophil depletion data suggest that neutrophils are significantly but not completely responsible for the therapeutic effects of RC NPs.

https://doi.org/10.1038/s41467-024-52812-6

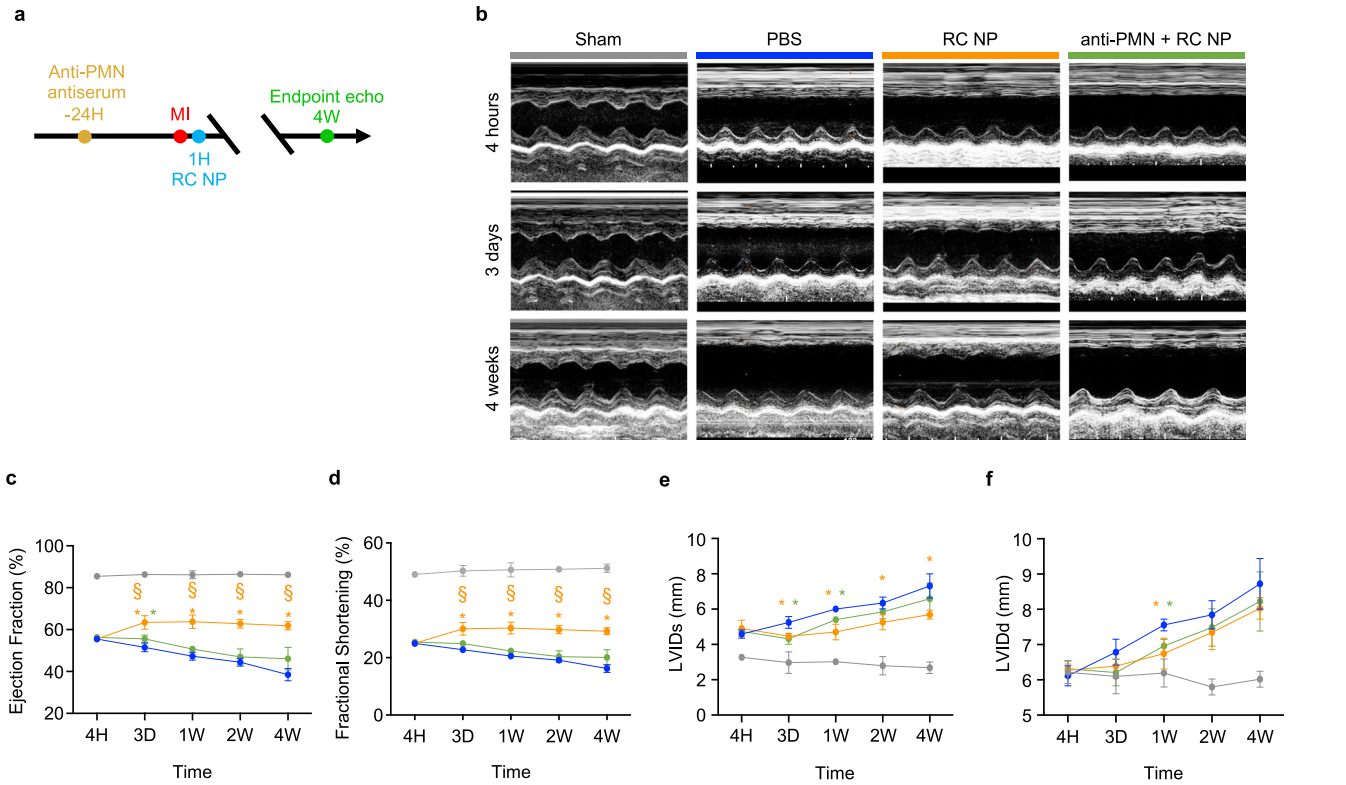

Fig. 9 | Reduced efficacy of RC NPs upon polymorphonucleocyte depletion. **a** Experimental timeline for neutrophil depletion and analysis of therapeutic efficacy. **b** Representative M-mode images at various time points post-MI. **c** Left ventricular ejection fraction, (**d**) fractional shortening, (**e**) LVIDs, and (**f**) LVIDd of rats at indicated time points ($n = 3$ for sham, 5 for other groups). $^{*}p < 0.05$ vs PBS; $^{§}p < 0.05$ vs anti-PMN + RC NP. All data presented as mean ± SD. Two-way ANOVA was used for all comparisons.

Biocompatibility of RC NPs

As indiscriminate neutrophil killing can cause neutropenia which increases vulnerability to pathogens, we measured the levels of circulating neutrophils after MI and found that RC NPs had no effect on circulating neutrophils (Fig. 10a, Supplementary Fig. 14a, b). RC NPs significantly reduced cardiac neutrophil counts 3 days after MI (Fig. 10b), which may be due to the cardioprotective properties of RC NPs. As RC NPs largely accumulate in the liver and spleen, we screened for potential long-term cell cycle arrest or apoptosis in the livers and spleens of uninjured rats. RC NP treatment did not induce significant long-term cell cycle arrest (Fig. 10c, Supplementary Fig. 15) nor did RC NP treatment alter the mRNA expression of apoptosis regulatory proteins *Bax*, *Bcl2*, and *Bclxl* in the livers and spleens of uninjured rats (Fig. 10d). Histological analysis showed that RC NPs did not induce discernable toxicity in major organs (Fig. 10e). We found that blood chemistry profiles were not affected by RC NP injection in both uninjured and MI rats, except for significantly lower serum lactate dehydrogenase (LDH; an indicator of tissue damage) levels in RC NP-treated animals 3 days post-MI (Supplementary Figs. 14 and 16). This may be another indication of potential cardioprotection conferred by RC NPs. Therefore, although RC NPs accumulate in other major organs apart from the heart, its accumulation results in no significant side effects (Fig. 10, Supplementary Figs. 14–16), perhaps due to the slower and more sustained rate of drug release in non-ROS conditions. As the toxicity of Free R-treated uninjured and MI rats were also similar to that of both NT and RC NP-treated uninjured and MI rats (Supplementary Figs. 14 and 16), it is possible that the lack of evident toxicity in RC NP-treated rats could also be due to the moderate doses of roscovitine used in our in vivo studies. Collectively, our results suggest that RC NPs are neutrophil-tropic, specific, and accumulate in infarcted hearts without discernable side effects.

Discussion

Increased access to medical care and technological advances in cardiology have improved mortality following MI, but morbidity remains a profound problem[1]. MI affects over 7 million individuals worldwide each year but as of present, there is no effective intervention to recover injured myocardium or mitigate LV cardiac remodeling[1,62]. As our understanding of the immunopathogenesis underlying MI grows, so does the opportunity for novel therapeutic strategies[63,64]. The CANTOS trial, which showed that the IL-1β-blocking antibody canakinumab significantly lowers the rate of recurrent atherosclerosis-related cardiovascular events, highlights the exciting potential of immunotherapy for cardiovascular diseases[65]. Here, we showed that nanoimmunotherapy targeting neutrophils in a spatiotemporal manner has therapeutic potential for the most lethal manifestation of cardiovascular disease, MI.

RC NP therapy has significant advantages over regenerative strategies for MI. Since the adult heart has little to no inherent ability for repair or regeneration[66], RC NP-mediated cardioprotection which mitigates largely irreversible MI injury could be advantageous over strategies that aim at repairing the damaged and fibrotic heart. Regenerative strategies such as stem cell therapies for MI are complicated by poor engraftment, non-off-the-shelf properties, and limited clinical benefits[67–70]. In contrast, RC NPs are off-the-shelf and exert their cardioprotective and healing effects after intravenous injection by leveraging the intrinsic neutrophil response to MI. Generation of autologous de novo cardiomyocytes ex vivo by fibroblast reprogramming to replace apoptotic cardiomyocytes after MI is expensive, complicated, and subject to variability[71]. The RC NP fabrication process is relatively inexpensive, facile, and results in homogenous nanoparticles. miRNA-based regenerative strategies are marred by the difficulty of delivering therapeutically relevant doses of miRNA to the heart and potent side effects[72,73]. RC NPs in contrast accumulate in

https://doi.org/10.1038/s41467-024-52812-6

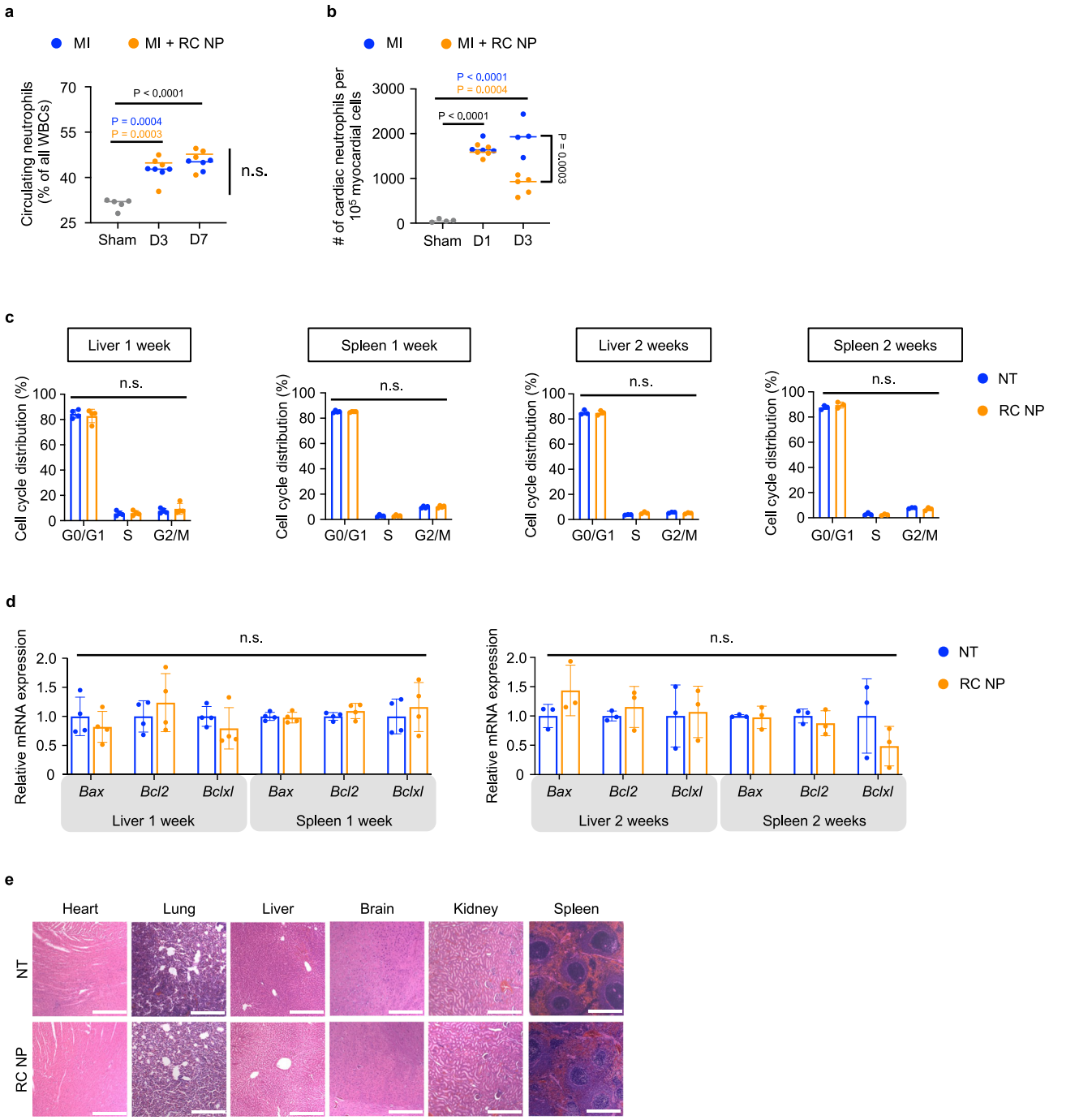

Fig. 10 | Toxicity evaluation of RC NPs. a Percentage of circulating neutrophils in sham and MI rats shows no evidence of RC NP-induced neutropenia ($n = 4$ for all MI groups, 5 for sham). **b** Number of cardiac neutrophils per 10^5 myocardial cells in sham and MI rats (with or without RC NP intervention) 1 and 3 days post-MI determined using flow cytometry ($n = 4$ for sham, MI + PBS D1/D3, and 5 for MI + RC NP D1/D3). **c** Percentage of cells in G0/G1, S, and G2/M phases in the livers and spleens of uninjured rats 1 and 2 weeks after RC NP injection ($n = 3$ for liver/spleen at 2 weeks, and 4 liver/spleen at 1 week). **d** Relative mRNA expression of apoptosis regulatory proteins *Bax*, *Bcl2*, and *Bclxl* in the livers and spleens of uninjured rats 1 and 2 weeks after RC NP injection ($n = 3$ for liver/spleen at 2 weeks, and 4 liver/spleen at 1 week). n.s., not significant. **e** Representative H&E-stained histological sections of major organs 14 days after RC NP injection in healthy F344 rats ($n = 3$). Scale bars, 100 μm. All data presented as mean ± SD. One-way ANOVA was used for comparisons in **a** and **b**. Multiple unpaired two-sample *t* tests were used for the comparison in **c**. Unpaired two-sided *t* tests were used for the comparisons in **d**.

infarcted hearts at therapeutically relevant doses without discernable side effects (Figs. 5–10).

RC NPs directly modulate the activation and death of neutrophils and through neutrophil modulation, influence macrophage phenotypes during the early stages of MI (Fig. 6). The early stage of MI is typically regarded as the first 72 h after MI, and is characterized by massive cardiomyocyte death and neutrophil infiltration[74,75]. As RC NPs modulate mainly neutrophils, we anticipate that the therapeutic effects of RC NPs would be diminished if RC NPs were administered during the late stages of MI, which occur for weeks after the early stage and is characterized by lower levels of pro-inflammatory infiltrating neutrophils[74,75].

Conventional neutrophil targeting strategies are relatively one-dimensional as they indiscriminately downregulate neutrophil activity

and sacrifice neutrophil-regulated healing at the injury site. In contrast, RC NPs are capable of both downregulating overexuberant neutrophil signaling and promoting neutrophil-mediated repair. This can be ascribed to the unique characteristics of RC NPs. RC NPs are readily taken up by circulating and cardiac neutrophils (Fig. 5a, b, f). After uptake, RC NPs induce apoptosis in cardiac neutrophils in infarcted hearts (Fig. 6a) as RC NPs are able to rapidly release roscovitine in H_2O_2 conditions (Fig. 2f). RC NP-induced apoptotic neutrophils can promote macrophage efferocytosis (Fig. 4a, b). Following efferocytosis, cardiac macrophages are polarized to the M2 phenotype (Fig. 6c–e, Supplementary Fig. 9). As RC NPs release roscovitine in unactivated neutrophils and non-H_2O_2 conditions more slowly than in H_2O_2 conditions (Fig. 2f), RC NPs would not induce aberrant neutrophil apoptosis in organs apart from the infarcted heart, or induce other forms of toxicity (Fig. 10, Supplementary Figs. 14–16). To validate the clinical viability of RC NPs, further testing in more diverse preclinical models is required as the population and phenotypes of neutrophils are known to differ between rodents and humans, males and females, and oscillate between day and night[76–78]. Further analysis of potential side effects such as complement activation are also warranted due to the non-stealth nature of RC NPs[79].

Roscovitine has shown safety but low efficacy in clinical trials dealing with advanced malignancies. With growing evidence that roscovitine exerts its effects by inducing neutrophil apoptosis[28,80–82], roscovitine has reentered clinical trials targeting inflammatory diseases such rheumatoid arthritis[83] and Cushing's disease[84]. Our data suggest that roscovitine in its soluble form has therapeutic potential for the treatment of MI and that RC NPs can provide more powerful and precise control over neutrophil fate than roscovitine alone (Figs. 6–8). We anticipate that our work will contribute to the development of multifaceted neutrophil targeting treatments for neutrophil-mediated inflammatory diseases.

Methods

Nanoparticle preparation

RC NPs were prepared using the water-in-oil-in-water double emulsion method. The aqueous phase was prepared by dissolving 2.3 mg of catalase (Sigma-Aldrich, St. Louis, MO, USA) in 1 ml of 10 mg/ml poly(vinyl alcohol) (PVA; molecular weight ~31,000, Sigma-Aldrich) solution. The organic phase was prepared by dissolving 45 mg of PLGA (acid terminated, molecular weight 7000–17,000, Sigma-Aldrich) and 8 mg of roscovitine (MedChemExpress, Monmouth Junction, NJ, USA) in 2 ml of dichloromethane (Sigma-Aldrich). The aqueous phase was added dropwise to the organic phase and ultrasonicated (Branson Sonifier, Branson Ultrasonic, CA, USA) for 10 s in an ice bath. For fluorescence experiments, DiO or DiI or DiD (Sigma-Aldrich for DiO; Thermo Fisher, Waltham, MA, USA for DiI and DiD) was dissolved in dichloromethane together with PLGA and roscovitine. The primary emulsion was then added dropwise to 6 ml of 20 mg/ml PVA solution and ultrasonicated for 40 s on ice at 10 s intervals to create the double emulsion. The resulting emulsion was diluted in 20 ml of distilled water, stirred for 4 h, and washed thrice with distilled water. After the final wash, RC NPs were resuspended in 0.4 ml of PBS and dialyzed against PBS before use.

Nanoparticle characterization

Roscovitine content in RC NPs was determined using high-performance liquid chromatography (HPLC; Agilent 1260 Infinity II LC System, CA, USA) after dissolving RC NPs in DMSO (Sigma-Aldrich). Size and morphology of RC NPs were ascertained using dynamic light scattering (DLS; Zetasizer Nano ZS, Malvern Panalytical, Malvern, UK), field emission-transmission electron microscopy (JEM-F200, JEOL Ltd, Tokyo, Japan), and field emission-scanning electron microscopy (JSM-7800F Prime, JEOL Ltd, Tokyo, Japan) installed at the National Center for Inter-university Research Facilities (NCIRF) at Seoul National University. Size stability was determined using DLS with RC NPs resuspended in either PBS or 50% FBS and incubated at 37 °C. Oxygen generation by RC NPs upon the addition of 50 mM of H_2O_2 was measured every 30 s using a dissolved oxygen meter (HI9136, HANNA instruments, Seoul, Republic of Korea). Roscovitine release was evaluated by dialyzing RC NPs (molecular weight cutoff 3500) in 35 ml of PBS with or without 100 or 200 μM H_2O_2 and incubating samples at 37 °C with shaking (100 rpm). Samples were removed at indicated intervals, and roscovitine concentrations were determined using HPLC. The Amplex™ Red Hydrogen Peroxide/Peroxidase Assay Kit (Thermo Fisher) was used to determine the amount of H_2O_2 remaining after reaction with nanoparticles. 50 μL of H_2O_2 (diluted in 1× reaction buffer) was mixed with 10 μL of nanoparticles (or PBS) and incubated at room temperature for 5 min before addition of 50 μL of working solution consisting of Amplex™ Red Reagent and horseradish peroxidase. Fluorescence was measured using a fluorescence microplate reader. Amplex Red intensity values were subtracted from average intensity values at 0 μM H_2O_2.

Animals

All animal studies were approved by the Institutional Animal Care and Use Committee (IACUC) of The Catholic University of Korea (Approval number: CUMC-2022-0081-02). The IACUC and Department of Laboratory Animals (DOLA) at Catholic University of Korea, Songeui Campus accredited the Korea Excellence Animal Laboratory Facility from Korea Food and Drug Administration in 2017 and acquired AAALAC International full accreditation in 2018. All animal procedures conformed to the guidelines from Directive 2010/63/EU of the European Parliament on the protection of animals used for scientific purposes or the NIH guidelines. F344 rats (male, 8–11 weeks old) were purchased from KOATECH (Gyeonggi. Republic of Korea) and BALB/c mice (female, 6–10 weeks old) were purchased from JA Bio (Gyeonggi, Republic of Korea). Animals were kept under a 12 h light and dark cycle, with temperatures ranging between 20 and 24 °C, and humidity between 45 and 55%. All animals were allowed to acclimatize for 1 week prior to experimentation.

Bone marrow-derived neutrophil and macrophage isolation

Neutrophils and macrophages were derived from the bone marrows of mice as previously described[12,85]. To isolate neutrophils, bone marrow cells were extracted from the tibias and femurs of mice, layered on top of 3 mLs of Histopaques 1077 and 1119 (Sigma-Aldrich), centrifuged for 30 min at 1000 × g without braking, and obtained at the interface between the two layers. Neutrophils were washed with PBS and allowed to rest in wells for one hour before use. For macrophages, bone marrow cells were extracted from the tibias and femurs of mice and differentiated for five days in M-CSF (25 ng/ml; Biolegend, San Diego, CA, USA) 10% FBS (Thermo Fisher) DMEM High medium (Thermo Fisher). For in vitro experiments, neutrophils were cultured in 3% FBS RPMI medium (Thermo Fisher) while macrophages were cultured in 10% FBS DMEM High medium. Bone marrow-derived neutrophils were defined as $CD11b^+Ly6G^+$ while bone marrow-derived macrophages were defined as $F4/80^+$. Purity exceeded 90% for both cells. Anti-mouse/human CD11b, anti-mouse Ly6G, and anti-mouse F4/80 antibodies were purchased from Biolegend.

RC NP uptake by neutrophils in vitro

Isolated neutrophils were treated with RC NPs containing 20 μM roscovitine and internalization was assessed one hour later by flow cytometry and two hours later by confocal microscopy. For flow cytometry experiments, 5×10^5 neutrophils were seeded on untreated 12-well cell culture dishes (Corning, NY, USA), treated with DiO-labeled RC NPs, and RC NP^+ neutrophils were analyzed using a FACSCanto™ II system (BD Biosciences, Franklin Lakes, NJ, USA) and FlowJo™ software (Tree Star Inc., Ashland, OR, USA). For confocal experiments, 2.5×10^5

neutrophils were seeded on poly-L-lysine (Thermo Fisher)-coated 4-well cell culture slides (SPL Life Sciences, Gyeonggi, Republic of Korea) and treated with DiI-labeled RC NPs. Neutrophils were washed with Hank's Balanced Salt Solution (HBSS; Thermo Fisher), stained with 5 μg/ml of 488 Wheat Germ Agglutinin (WGA; Thermo Fisher) for 10 min at 37 °C, washed with HBSS, fixed with 4% paraformaldehyde for 15 min, washed with HBSS, and counterstained with 4′6-diamidino-2-pheylindole (DAPI, Vector Laboratories, Burlingame, CA, USA). Cells were visualized by confocal microscopy (Stellaris 8; LEICA, Wetzlar, Germany). Unless stated otherwise, all immunofluorescence experiments were conducted on 4-well cell culture slides. All chemical probes used in our experiments comply with the criteria specified by the Chemical Probes Portal.

Viability and physiology of RC NP$^+$ neutrophils in vitro

NETosis and viability of RC NP$^+$ neutrophils were determined using SYTOX Green (Thermo Fisher) and Zombie Violet (Biolegend) staining, respectively, 3 and 6 h after RC NP (20 μM) treatment. Fluorescence intensity of SYTOX Green-stained NETting neutrophils was measured using a fluorescence microplate reader (Sunrise™; Tecan, Männedorf, Switzerland) while nonviable Zombie Violet$^+$ neutrophils were analyzed using flow cytometry. Chemotaxis of RC NP$^+$ neutrophils was investigated using a transwell migration assay (polycarbonate membrane, 3.0 μm pore size, 6.5 mm diameter, and 0.33 cm^2 surface area) (Corning). Neutrophils (2.5×10^5 cells per well) treated with different concentrations of RC NPs were added to the upper chambers of transwells. Lower chambers were filled with 1 μM of fMLP and after 1 h of incubation at 37 °C, neutrophils in the lower chambers were counted using a hemacytometer. To verify fMLP-induced neutrophil chemotaxis, neutrophils were seeded in transwells as described above, with 1 μM of fMLP in lower chambers, and neutrophils in the lower chambers were counted after one hour of incubation.

In vitro neutrophil activation

Isolated neutrophils were pretreated with 50 μM of RC NPs or free drugs for two hours before PMA activation (750 nM). Cell culture supernatants, NETosis, and apoptosis were analyzed 15 h after PMA activation. TNF-α (Biolegend), pro-MMP-9 (Thermo Fisher), and neutrophil elastase (R&D Systems, Minneapolis, MN, USA) ELISA were used according to the manufacturer's instructions to determine relevant protein concentrations in supernatants. NETs were stained using SYTOX Green, visualized by confocal microscopy, and quantified using ImageJ software (National Institutes of Health, NY, USA). NET area was defined as SYTOX Green$^+$DAPI$^-$ area. Apoptosis was detected by TUNEL (Promega, Madison, WI, USA) staining according to the manufacturer's instructions, visualized by confocal microscopy, and quantified using ImageJ software. DAPI served as a counterstain for both NETosis and apoptosis experiments. For ELISA experiments, 5×10^5 neutrophils were seeded on untreated 12-well cell culture dish plates. For confocal microscopy experiments, 2.5×10^5 neutrophils were seeded on poly-L-lysine-coated 4-well cell culture slides.

Neutrophil and macrophage coculture

Neutrophils (5×10^5) were pretreated with nanoparticles or free drugs before PMA activation as described earlier. After 15 h, neutrophils were collected and washed twice with PBS to remove residual RC NPs. 5×10^5 neutrophils were added to wells containing 1×10^5 macrophages with 1 ng/ml of LPS (Thermo Fisher). For flow cytometry efferocytosis experiments, neutrophils were stained immediately after isolation with DiD according to the manufacturer's instructions and macrophage efferocytosis of apoptotic neutrophils was identified as F4/80$^+$DiD$^+$ events. Percent efferocytosis was then normalized to the PBS group. Flow cytometry efferocytosis experiments were conducted 20 min after coculture. For confocal-based observation of efferocytosis, 2.5×10^5 neutrophils were stained with DiI and 0.5×10^5 macrophages were stained with Alexa Fluor™ 488 WGA, both according to the manufacturer's instructions. After 40 min of coculture, non-phagocytosed neutrophils were washed away using PBS and samples were fixed with 4% PFA for 15 min. Cells were counterstained with DAPI and visualized by confocal microscopy.

For assessment of macrophage polarization after coculture, neutrophils and macrophages were cultured as described above. Macrophages were analyzed by flow cytometry 24 h into coculture. Anti-mouse F4/80, anti-mouse CD80, and anti-mouse CD86 antibodies were purchased from Biolegend. For qRT-PCR, ICC, and ELISA experiments, neutrophils were removed from coculture by vigorous pipetting and macrophage phenotypes were allowed to further develop for another 16 h. For ICC experiments, macrophages were stained with WGA prior to coculture. After coculture, cells were fixed with 4% PFA for 10 min, washed with ice-cold PBS, and permeabilized with 0.1% Triton X-100 if necessary. Samples were blocked with 10% goat serum in PBS overnight at 4 °C, washed with PBS, incubated in secondary antibody diluted with 10% goat serum for 1 h at room temperature, washed with PBS, and counterstained with DAPI. Cells were visualized by confocal microscopy and quantified using ImageJ software. For qRT-PCR, F4/80$^+$ macrophages were sorted by flow cytometry and total RNA was isolated from macrophages using Trizol™ (Qiagen, Valencia, CA, USA). cDNAS were prepared using AccuPower® RT Master Mix (Bioneer, Daejeon, Korea) and SYBR Green-based qRT-PCR was performed using TOPreal™ qPCR 2x Premix (Enzynomics, Daejaeon, Korea). The list of primer sequences used in this study can be found in Supplementary Table 1. For ELISA experiments, cell supernatants were collected, centrifuged at $1000 \times g$ for 10 min, and stored at −80 °C till further analysis. TNF-α, IL-12 p40, IL-6 ELISA kits were obtained from Biolegend. TGF-β1 ELISA kit was obtained from Thermo Fisher.

Biodistribution and in vivo nanoparticle uptake

To determine relative nanoparticle uptake by neutrophils and monocytes, DiO-labeled RC NPs (200 μl; 2 mg/kg of roscovitine) were intravenously injected into tail veins of BALB/c mice. At indicated time points after injection after injection, blood was drawn by retroorbital bleeding into heparin-coated syringes. Red blood cells were lysed using Gibco™ ACK Lysing Buffer (Thermo Fisher) according the manufacturer's instructions. Samples were incubated with 100 μg/ml of IgG (Invitrogen) for 15 min at 4 °C for our FACS experiments prior to staining with fluorescence-conjugated antibodies to prevent non-specific binding. Leukocytes were then stained with fluorescence-conjugated antibodies for 30 min at 4 °C. Anti-mouse CD45, anti-mouse/human CD11b, anti-mouse Ly6G, and anti-mouse Ly6C antibodies were purchased from Biolegend. To determine RC NP uptake by neutrophils in rat hearts, DiD-labeled RC NPs (400 μl; 2 mg/kg of roscovitine) were intravenously injected into tail veins of either sham or MI rats. 24 h after injection, hearts were dissected with perfusion, minced, and digested with 2 mg/ml of Collagenase Type IV (Worthington Biochemical, Lakewood, NJ, USA) and 1.2 U/ml of Dispase II (Sigma-Aldrich) in RPMI medium. Heart tissues were homogenized using a gentleMACS™ Dissociator (Miltenyl Biotec, Bergisch-Gladbach, Germany) and filtered through a 100 μm cell strainer. Cell suspensions were washed with PBS and flow cytometry staining buffer before subsequent staining and analysis. Anti-rat CD45, CD43, CD161, and CD3 antibodies were purchased from Biolegend and anti-rat His48, CD43, and B220 antibodies were purchased from Invitrogen. Rat leukocytes were gated as previously described[86]. To determine RC NP distribution in major organs, sham and MI rats were intravenously injected with DiD-labeled RC NPs (400 μl; 2 mg/kg of roscovitine). 24 h after injection, hearts, lungs, livers, brains, kidneys, and spleens were removed and imaged using an IVIS® Spectrum In Vivo Imaging System (PerkinElmer, Waltham, MA, USA).

Pharmacokinetics
RC NPs were labeled with the near-IR dye DiR (Thermo Fisher) and intravenously injected into the tail veins of uninjured rats. Blood was sampled 3 min, 20 min, 45 min, 6 h, 24 h, 48 h, and 72 h after RC NP injection. Samples were diluted 10x in PBS and fluorescence intensity was measured using an absorbance microplate reader (Sunrise™; Tecan, Männedorf, Switzerland). Blood from non-treated rats was also sampled and measured to account for background fluorescence.

In vivo toxicity assessment
To evaluate potential in vivo toxicity, RC NPs were intravenously injected into (400 μl; 2 mg/kg of roscovitine) uninjured and MI rats. Whole blood was collected by retroorbital bleeding from uninjured rats immediately before injection and 3, 10, and 14 days after injection. Serum was collected by centrifugation and serum levels of AST, ALT, albumin (ALB), total bilirubin (TBIL), BUN, and CRE were measured using a chemistry analyzer (DRI-CHEM 3500S 19; Fujifilm, Tokyo, Japan). Whole blood was collected by retroorbital bleeding from MI rats 1 and 3 days after RC NP injection. Serum levels of AST, ALT, BUN, CRE, TBIL, ALB, and LDH were measured using a chemistry analyzer and neutrophil counts were measured using a veterinary hematology system (Hemavet 950; Drew Scientific Inc., Miami Lakes, FL, USA). For histological analysis, major organs were harvested 14 days after RC NP injection in uninjured rats, fixed with 4% PFA in PBS, and constructed into paraffin blocks. Samples were sectioned at a thickness of 5 μm using a microtome (RM2125RT, Leica, Germany), stained with H&E, and imaged using an optical microscope (IX71, Olympus, Tokyo, Japan). For cell cycle analysis, livers and spleens were minced, digested with 2 mg/ml of Collagenase Type IV and 1.2 U/ml of Dispase II in serum-free RPMI medium and homogenized using a gentleMACS™ Dissociator. Single-cell suspensions were filtered through a 100 μm cell strainer, washed twice with PBS, and fixed in ice-cold 70% ethanol for 30 min at 4 °C. After fixation, cells were washed twice, treated with RNase (Sigma-Aldrich) and strained with propidium iodide (PI) (Biolegend) 15 min before FACS analysis. To screen for potential apoptosis in the liver and spleen, single-cell suspensions were prepared as described above and RNA was isolated using Trizol™. cDNAs were prepared using AccuPower® RT Master Mix and SYBR Green-based qRT-PCR was performed using TOPreal™ qPCR 2x Premix. The list of primer sequences used in this study can be found in Supplementary Table 1.

Determination of infarct size
EB and TTC chloride staining was performed to determine infarct size. 24 h after MI, the suture thread around the LAD artery was retied, and EB dye (7% in PBS) was injected intravenously into the rats. After 1 min, the heart was quickly excised and incubated for 10 min at −4 °C. The heart was cut into 3 slices (each one approximately 2 mm thick) and incubated with 2% TTC for 30 min at 37 °C in the dark. After being washed three times, the tissue was fixed in 4% paraformaldehyde. The non-infarcted myocardium was stained deep blue with EB. The viable myocardium was stained red with TTC. The infarcted myocardium appeared white after TTC staining. The area at risk (AAR) and the infarcted area were determined digitally by ImageJ.

MI model and nanoparticle treatment
Male F344 rats (8–10 weeks old) were anesthetized with 2% inhaled isoflurane and intubated via the trachea with an 18-gauge intravenous catheter. The rats were then mechanically ventilated with a rodent respirator (55-7058, Harvard Apparatus, Canada, USA). Animals were placed on a 37 °C heating pad to prevent cooling during the procedure. After shaving the chest and sterilizing with 70% alcohol, left thoracotomy was performed. MI was induced by occluding the left anterior descending (LAD) artery with a 7–0 Prolene suture for 1 hr. The nanoparticles and roscovitine were diluted with PBS (400 μl; 2 mg/kg of roscovitine) and intravenously injected immediately before reperfusion. The chest was closed aseptically and cefazolin (10 mg/kg) and ketoprofen (3 mg/kg) were administered before and after surgery. Alternating group randomization was conducted during the operational window and all experiments were conducted at a similar time of day to minimize the influence of circadian rhythms.

Neutrophil depletion
Rats were intravenously injected with 0.3 mL of anti-PMN antiserum (host, rabbit) (Cat #A51140, Accurate Chemical & Scientific, Westbury, NY) 24 h before MI. Non-depleted rats received equal volumes of normal rabbit serum (Cat #JNZ000120, Accurate Chemical & Scientific, Westbury, NY).

Echocardiography
Animals were lightly anesthetized with isoflurane and maintained at 37 °C using a heating pad. Heart function in MI rats were analyzed with echocardiography. Physiological data was recorded using a transthoracic echocardiography system equipped with a 15 MHz L15-7io linear transducer (Affniti 50 G, Philips, Amsterdam, Netherlands). To establish baseline LV function, we performed echocardiography 4 h post-MI (inclusion criterion: ejection fraction <58% based on echocardiographic evaluation). After baseline (4 h) echocardiography, serial echocardiography was conducted 3 days, 1 week, 2 weeks, and 4 weeks post-MI. The echocardiography operator was blinded to group allocations during the experiment.

Cardiac strain analysis
Global circumferential strain was derived parasternal short-axis views, recorded using a transthoracic echocardiography system equipped with an 11.0 MHz 12S-RS Sector Probe (Vivid™ iq, GE Healthcare, Chicago, IL, USA). Sampling points were manually placed along the epicardial and endocardial layers during the end-systolic period. Using GE EchoPAC v204 software, tissue speckles were identified and tracked throughout the cardiac cycle on a frame-by-frame basis, allowing the calculation of the global circumferential strain.

Hemodynamic measurements
Hemodynamic measurements were conducted 4 weeks post-MI. After thoracotomy without bleeding, the LV apex of the heart was punctured with a 26-gauge needle, and a 2 F conductance catheter (SPR-838, Millar) was inserted into the LV. LV pressure-volume parameters were continually recorded using a PV conductance system (MPVS Ultra, EMKA Technologies, Paris, France) coupled to a digital converter (PowerLab 16/35, ADInstruments, Colorado Springs, CO, USA). Load-independent measurements of cardiac function, including the slopes ESPVR and EDPVR, were obtained with different preloads, which were elicited via transient inferior vena cava occlusion with a needle holder. An aliquot of 50 μl of hypertonic saline (20% NaCl) was injected into the left jugular vein to calculate the parallel conductance after hemodynamic measurements. The blood was collected from the left ventricle into a heparinized syringe and placed into cuvettes to convert the conductance signal to volume using the catheter. The absolute volume of the rat was defined by calibrating the parallel conductance and the cuvette conductance.

Determination of fibrosis
Infarcted hearts 4 weeks post-MI were fixed in 4% PFA and constructed into paraffin blocks for Masson's trichrome (Sigma-Aldrich) staining to determine circumferential fibrosis and viable myocardium. Briefly, paraffin slides were preincubated in a 37 °C dry oven before deparaffinization and rehydration. The paraffin sections were then refixed for one hour in 56 °C Bouin's solution, stained using Weigert's iron hematoxylin solution for 15 min at room temperature, and further stained with Biebrich scarlet-acid fuchsin solution for 20 min at room

temperature. Finally, the sections were counterstained with aniline blue for 15 min, followed by 1% acetic acid incubation for 1 min at room temperature. Extensive washes were performed between each step. Subsequently, heart sections were imaged using a slide scanner (Pannoramic MIDI, Budapest, Hungary). The percentage of fibrosis was calculated as the area of fibrosis to the area of LV circumference [(infarct area/LV wall area) × 100]. The percentage of viable myocardium was defined as the area of myocardium within the infarct area where the LV wall is dilated, and the fibrotic area is exhibited. [(myocardium area/infarct area) × 100]. Both measurements were performed using ImageJ software.

Immunohistochemistry

At the time of sacrifice, the hearts were fixed in 4% PFA overnight and constructed into paraffin blocks. The heart was cross-sectioned into 5 µm sections starting at the top of the apex using a microtome (RM2255; Leica). After deparaffinization and rehydration, antigen retrieval with target retrieval solution (DAKO, Santa Clara, CA, USA) was performed. The sections were incubated with diluted primary antibody at 4 °C overnight. The primary antibodies used in this study were mouse anti-cTnT (Abcam, Cambridge, UK; 1:200), goat anti-CD31 (Novus, St. Louis, MO, USA; 1:200), rabbit anti-MPO (Boster Bio, Pleasanton, CA, USA; 1:200), mouse anti-CD68 (Abcam; 1:200), rabbit anti-iNOS (Abcam; 1:200), rabbit anti-CD206 (Abcam; 1:200), rabbit anti-Arg1 (Novus Biologicals; 1:300). After washing three times with 1% Tween 20 in PBS, the samples were incubated with secondary antibody for 90 min at room temperature in the dark. The secondary antibodies used in this study were anti-mouse Alexa Fluor 594 (Invitrogen, Waltham, MA, USA; 1:500), anti-mouse Alexa Fluor 647 (Invitrogen; 1:500), anti-goat Alexa Fluor 488 (Invitrogen; 1:500), anti-goat Alexa Fluor 594 (Invitrogen; 1:500), anti-rabbit Alexa Fluor 488 (Invitrogen; 1:500). After washing thrice with PBS, the sections were stained with DAPI mounted on slides. The stained sections were assessed using a fluorescence microscope. Operators were blinded to groups during acquisition and quantification of all image-based assays.

Cardiac leukocyte analysis

Hearts were dissected with perfusion, minced, and digested with 2 mg/ml of Collagenase Type IV and 1.2 U/ml of Dispase II in RPMI medium. Heart tissues were homogenized using a gentleMACS™ Dissociator and filtered through a 100 µm cell strainer. Samples were incubated with 100 µg/ml of anti-mouse IgG (Invitrogen) for 15 min at 4 °C to prevent nonspecific binding. Cell suspensions were then stained with Zombie NIR (Biolegend) for 15 min at room temperature. Afterwards, cell suspensions were incubated at 4 °C with fluorophore-conjugated antibodies. Anti-rat CD45, CD68, CD3, and CD86 antibodies were purchased from Biolegend, anti-rat His48 antibody was purchased from Invitrogen, and anti-rat CD80 antibody was purchased from BD Biosciences. Tru-Nuclear™ Transcription Factor Buffer Set (Biolegend) was used according to the manufacturer's instructions when permeabilization was required.

Statistical analysis

All quantitative data are presented as the mean ± SD unless otherwise indicated. Differences between two groups were analyzed by two-tailed Student's *t* tests. Differences between groups were analyzed by one-way ANOVA with Bonferroni's post-hoc analysis. Differences between groups over multiple time points were analyzed by two-way ANOVA with Bonferri's correction. Results were considered statistically significant when $p < 0.05$.

Reporting summary

Further information on research design is available in the Nature Portfolio Reporting Summary linked to this article.

Data availability

The authors declare that all data needed to support the findings of this study are presented in the Article, Supplementary Information, and Source Data file. Source data are provided with this paper.

References

1. Reed, G. W., Rossi, J. E. & Cannon, C. P. Acute myocardial infarction. *Lancet* **389**, 197–210 (2017).
2. Anderson, J. L. & Morrow, D. A. Acute myocardial infarction. *N. Engl. J. Med.* **376**, 2053–2064 (2017).
3. Vafadarnejad, E. et al. Dynamics of cardiac neutrophil diversity in murine myocardial infarction. *Circ. Res.* **127**, e232–e249 (2020).
4. Puhl, S.-L. & Steffens, S. Neutrophils in post-myocardial infarction inflammation: damage vs. resolution? *Front. Cardiovasc. Med.* **6**, 25 (2019).
5. Soehnlein, O., Steffens, S., Hidalgo, A. & Weber, C. Neutrophils as protagonists and targets in chronic inflammation. *Nat. Rev. Immunol.* **17**, 248–261 (2017).
6. Ma, Y., Yabluchanskiy, A. & Lindsey, M. L. Neutrophil roles in left ventricular remodeling following myocardial infarction. *Fibrogenes. Tissue Repair* **6**, 1–10 (2013).
7. Ge, L. et al. Neutrophil extracellular traps in ischemia-reperfusion injury-induced myocardial no-reflow: therapeutic potential of DNase-based reperfusion strategy. *Am. J. Physiol. Heart Circ. Physiol.* **308**, H500–H509 (2015).
8. Alam, S. R., Newby, D. E. & Henriksen, P. A. Role of the endogenous elastase inhibitor, elafin, in cardiovascular injury: from epithelium to endothelium. *Biochem. Pharmacol.* **83**, 695–704 (2012).
9. Vinten-Johansen, J. Involvement of neutrophils in the pathogenesis of lethal myocardial reperfusion injury. *Cardiovasc. Res.* **61**, 481–497 (2004).
10. Nagareddy, P. R. et al. NETosis is required for S100A8/A9-induced granulopoiesis after myocardial infarction. *Arterioscler. Thromb. Vasc. Biol.* **40**, 2805–2807 (2020).
11. Batra, R. et al. IL-1β (interleukin-1β) and TNF-α (tumor necrosis factor-α) impact abdominal aortic aneurysm formation by differential effects on macrophage polarization. *Arterioscler. Thromb. Vasc. Biol.* **38**, 457–463 (2018).
12. Monteith, A. J., Miller, J. M., Maxwell, C. N., Chazin, W. J. & Skaar, E. P. Neutrophil extracellular traps enhance macrophage killing of bacterial pathogens. *Sci. Adv.* **7**, eabj2101 (2021).
13. Frangogiannis, N. G. Regulation of the inflammatory response in cardiac repair. *Circ. Res.* **110**, 159–173 (2012).
14. Greenlee-Wacker, M. C. Clearance of apoptotic neutrophils and resolution of inflammation. *Immunol. Rev.* **273**, 357–370 (2016).
15. Moon S., Hong J., Go S., Kim B.-S. Immunomodulation for tissue repair and regeneration. *Tissue Eng. Regen. Med.* **20**, 389–409 (2023).
16. Horckmans, M. et al. Neutrophils orchestrate post-myocardial infarction healing by polarizing macrophages towards a reparative phenotype. *Eur. Heart J.* **38**, 187–197 (2017).
17. Fadok, V. A. et al. Macrophages that have ingested apoptotic cells in vitro inhibit proinflammatory cytokine production through autocrine/paracrine mechanisms involving TGF-beta, PGE2, and PAF. *J. Clin. Investig.* **101**, 890–898 (1998).
18. Savchenko, A. S. et al. VWF-mediated leukocyte recruitment with chromatin decondensation by PAD4 increases myocardial ischemia/reperfusion injury in mice. *Blood* **123**, 141–148 (2014).
19. García-Prieto, J. et al. Neutrophil stunning by metoprolol reduces infarct size. *Nat. Commun.* **8**, 14780 (2017).
20. Pharmaceuticals N., Novartis. A. Safety, tolerability and efficacy study in chronic obstructive pulmonary disease (COPD) Patients With QBM076). https://ClinicalTrials.gov/show/NCT01972776 (2013).

21. O'Byrne, P. M. et al. Efficacy and safety of a CXCR2 antagonist, AZD5069, in patients with uncontrolled persistent asthma: a randomised, double-blind, placebo-controlled trial. *Lancet Respir. Med.* **4**, 797–806 (2016).
22. Jonsson, H., Allen, P. & Peng, S. L. Inflammatory arthritis requires Foxo3a to prevent Fas ligand–induced neutrophil apoptosis. *Nat. Med.* **11**, 666–671 (2005).
23. Mócsai, A. et al. Integrin signaling in neutrophils and macrophages uses adaptors containing immunoreceptor tyrosine-based activation motifs. *Nat. Immunol.* **7**, 1326–1333 (2006).
24. Mitroulis, I. et al. Leukocyte integrins: role in leukocyte recruitment and as therapeutic targets in inflammatory disease. *Pharmacol. Ther.* **147**, 123–135 (2015).
25. Bisso, P. W., Gaglione, S., Guimarães, P. P., Mitchell, M. J. & Langer, R. Nanomaterial interactions with human neutrophils. *ACS Biomater. Sci. Eng.* **4**, 4255–4265 (2018).
26. Park, J. et al. Intravascular innate immune cells reprogrammed via intravenous nanoparticles to promote functional recovery after spinal cord injury. *Proc. Natl. Acad. Sci.* **116**, 14947–14954 (2019).
27. Saito, E. et al. Designing drug-free biodegradable nanoparticles to modulate inflammatory monocytes and neutrophils for ameliorating inflammation. *J. Control. Release* **300**, 185–196 (2019).
28. Rossi, A. G. et al. Cyclin-dependent kinase inhibitors enhance the resolution of inflammation by promoting inflammatory cell apoptosis. *Nat. Med.* **12**, 1056–1064 (2006).
29. Benson, C. et al. A phase I trial of the selective oral cyclin-dependent kinase inhibitor seliciclib (CYC202; R-Roscovitine), administered twice daily for 7 days every 21 days. *Br. J. Cancer* **96**, 29–37 (2007).
30. Le Tourneau, C. et al. Phase I evaluation of seliciclib (R-roscovitine), a novel oral cyclin-dependent kinase inhibitor, in patients with advanced malignancies. *Eur. J. Cancer* **46**, 3243–3250 (2010).
31. Simon, S. I. & Schmid-Schönbein, G. Biophysical aspects of microsphere engulfment by human neutrophils. *Biophys. J.* **53**, 163–173 (1988).
32. Sun, X., Guo, S., Chung, C. S., Zhu, W. & Sun, S. A sensitive H2O2 assay based on dumbbell-like PtPd-Fe3O4 nanoparticles. *Adv. Mater.* **25**, 132–136 (2013).
33. Hyslop, P. A., Zhang, Z., Pearson, D. V. & Phebus, L. A. Measurement of striatal H2O2 by microdialysis following global forebrain ischemia and reperfusion in the rat: correlation with the cytotoxic potential of H2O2 in vitro. *Brain Res.* **671**, 181–186 (1995).
34. Papayannopoulos, V. Neutrophil extracellular traps in immunity and disease. *Nat. Rev. Immunol.* **18**, 134–147 (2018).
35. Avgoustakis, K. et al. PLGA–mPEG nanoparticles of cisplatin: in vitro nanoparticle degradation, in vitro drug release and in vivo drug residence in blood properties. *J. Control. Release* **79**, 123–135 (2002).
36. Lin, X., Yang, H., Su, L., Yang, Z. & Tang, X. Effect of size on the in vitro/in vivo drug release and degradation of exenatide-loaded PLGA microspheres. *J. Drug Deliv. Sci. Technol.* **45**, 346–356 (2018).
37. Mohammad, A. K. & Reineke, J. J. Quantitative detection of PLGA nanoparticle degradation in tissues following intravenous administration. *Mol. Pharm.* **10**, 2183–2189 (2013).
38. Yoo, J. & Won, Y.-Y. Phenomenology of the initial burst release of drugs from PLGA microparticles. *ACS Biomater. Sci. Eng.* **6**, 6053–6062 (2020).
39. Jain, G. K. et al. Mechanistic study of hydrolytic erosion and drug release behaviour of PLGA nanoparticles: influence of chitosan. *Polym. Degrad. Stab.* **95**, 2360–2366 (2010).
40. Rescignano, N. et al. In-vitro degradation of PLGA nanoparticles in aqueous medium and in stem cell cultures by monitoring the cargo fluorescence spectrum. *Polym. Degrad. Stab.* **134**, 296–304 (2016).
41. Tamani, F. et al. Mechanistic explanation of the (up to) 3 release phases of PLGA microparticles: diprophylline dispersions. *Int. J. Pharm.* **572**, 118819 (2019).
42. Hussein, A. S., Abdullah, N. & Ahmadun FlR. In vitro degradation of poly (D, L-lactide-co-glycolide) nanoparticles loaded with linamarin. *IET Nanobiotechnol.* **7**, 33–41 (2013).
43. Xue, J. et al. Neutrophil-mediated anticancer drug delivery for suppression of postoperative malignant glioma recurrence. *Nat. Nanotechnol.* **12**, 692–700 (2017).
44. Metzler, K. D., Goosmann, C., Lubojemska, A., Zychlinsky, A. & Papayannopoulos, V. A myeloperoxidase-containing complex regulates neutrophil elastase release and actin dynamics during NETosis. *Cell Rep.* **8**, 883–896 (2014).
45. Pendergrass, K. D. et al. Temporal effects of catalase overexpression on healing after myocardial infarction. *Circ Heart Fail.* **4**, 98–106 (2011).
46. Fuchs, T. A. et al. Novel cell death program leads to neutrophil extracellular traps. *J. Cell Biol.* **176**, 231–241 (2007).
47. Aoshiba, K., Yasui, S., Hayashi, M., Tamaoki, J. & Nagai, A. Role of p38-mitogen-activated protein kinase in spontaneous apoptosis of human neutrophils. *J. Immunol.* **162**, 1692–1700 (1999).
48. Fromen, C. A. et al. Neutrophil–particle interactions in blood circulation drive particle clearance and alter neutrophil responses in acute inflammation. *ACS Nano* **11**, 10797–10807 (2017).
49. Summers, C. et al. Neutrophil kinetics in health and disease. *Trends Immunol.* **31**, 318–324 (2010).
50. Goto, Y., Hogg, J. C., Suwa, T., Quinlan, K. B. & van Eeden, S. F. A novel method to quantify the turnover and release of monocytes from the bone marrow using the thymidine analog 5′-bromo-2′-deoxyuridine. *Am. J. Physiol. Cell Physiol.* **285**, C253–C259 (2003).
51. Martin, T. P. et al. Preclinical models of myocardial infarction: from mechanism to translation. *Br. J. Pharmacol.* **179**, 770–791 (2022).
52. Parker, H., Dragunow, M., Hampton, M. B., Kettle, A. J. & Winterbourn, C. C. Requirements for NADPH oxidase and myeloperoxidase in neutrophil extracellular trap formation differ depending on the stimulus. *J. Leukoc. Biol.* **92**, 841–849 (2012).
53. Singhal, A., Morris, V., Labhasetwar, V. & Ghorpade, A. Nanoparticle-mediated catalase delivery protects human neurons from oxidative stress. *Cell Death Dis.* **4**, e903–e903 (2013).
54. Xu, G. & McLeod, H. L. Strategies for enzyme/prodrug cancer therapy. *Clin. Cancer Res.* **7**, 3314–3324 (2001).
55. Heble, A. Y., Santelli, J., Armstrong, A. M., Mattrey, R. F. & Lux, J. Catalase-loaded silica nanoparticles formulated via direct surface modification as potential oxygen generators for hypoxia relief. *ACS Appl. Mater. Interfaces* **13**, 5945–5954 (2021).
56. Safary, A., Akbarzadeh Khiavi, M., Omidi, Y. & Rafi, M. A. Targeted enzyme delivery systems in lysosomal disorders: an innovative form of therapy for mucopolysaccharidosis. *Cell. Mol. Life Sci.* **76**, 3363–3381 (2019).
57. Kühl, A. A. et al. Aggravation of different types of experimental colitis by depletion or adhesion blockade of neutrophils. *Gastroenterology* **133**, 1882–1892 (2007).
58. Moxon-Emre, I. & Schlichter, L. C. Neutrophil depletion reduces blood-brain barrier breakdown, axon injury, and inflammation after intracerebral hemorrhage. *J. Neuropathol. Exp. Neurol.* **70**, 218–235 (2011).
59. Friedrich, V. et al. Reduction of neutrophil activity decreases early microvascular injury after subarachnoid haemorrhage. *J. Neuroinflamm.* **8**, 1–12 (2011).
60. Hilton, G. D., Stoica, B. A., Byrnes, K. R. & Faden, A. I. Roscovitine reduces neuronal loss, glial activation, and neurologic deficits after brain trauma. *J. Cereb. Blood Flow. Metab.* **28**, 1845–1859 (2008).
61. Jhou, R. S. et al. Inhibition of cyclin-dependent kinases by olomoucine and roscovitine reduces lipopolysaccharide-induced

inflammatory responses via down-regulation of nuclear factor κB. *Cell Prolif.* **42**, 141–149 (2009).
62. Kinsella, J. Taking heart-Cardiac transplantation past, present, and future (vol 355, pg 231, 2006). *N. Engl. J. Med.* **355**, 967–967 (2006).
63. Duivenvoorden, R. et al. Nanoimmunotherapy to treat ischaemic heart disease. *Nat. Rev. Cardiol.* **16**, 21–32 (2019).
64. Ko, G. R. & Lee, J. S. Engineering of immune microenvironment for enhanced tissue remodeling. *Tissue Eng. Regen. Med.* **19**, 221–236 (2022).
65. Ridker, P. M. et al. Antiinflammatory therapy with canakinumab for atherosclerotic disease. *N. Engl. J. Med.* **377**, 1119–1131 (2017).
66. Liu, B. et al. Cell type–specific microRNA therapies for myocardial infarction. *Sci. Transl. Med.* **13**, eabd0914 (2021).
67. Trounson, A. & McDonald, C. Stem cell therapies in clinical trials: progress and challenges. *Cell Stem Cell* **17**, 11–22 (2015).
68. Jung M. et al. Iron oxide nanoparticle-incorporated mesenchymal stem cells for Alzheimer's disease treatment. *Nano Lett.*, (2023).
69. Van Nguyen, T.-T., Vu, N. B. & Van Pham, P. Mesenchymal stem cell transplantation for ischemic diseases: mechanisms and challenges. *Tissue Eng. Regen. Med.* **18**, 587–611 (2021).
70. Munderere, R., Kim, S.-H., Kim, C. & Park, S.-H. The progress of stem cell therapy in myocardial-infarcted heart regeneration: cell sheet technology. *Tissue Eng. Regen. Med.* **19**, 969–986 (2022).
71. Cahill, T. J., Choudhury, R. P. & Riley, P. R. Heart regeneration and repair after myocardial infarction: translational opportunities for novel therapeutics. *Nat. Rev. Drug Discov.* **16**, 699–717 (2017).
72. Juliano, R. L. The delivery of therapeutic oligonucleotides. *Nucleic Acids Res.* **44**, 6518–6548 (2016).
73. Mirna Therapeutics I. Pharmacodynamics study of MRX34, MicroRNA liposomal injection in melanoma patients with biopsy accessible lesions). https://ClinicalTrials.gov/show/NCT02862145 (2016).
74. Zhao W., Zhao J., Rong J. Pharmacological modulation of cardiac remodeling after myocardial infarction. *Oxid. Med. Cell. Longev.* **2020**, 8815349 (2020).
75. Yan, X. et al. Temporal dynamics of cardiac immune cell accumulation following acute myocardial infarction. *J. Mol. Cell. Cardiol.* **62**, 24–35 (2013).
76. Mestas, J. & Hughes, C. C. Of mice and not men: differences between mouse and human immunology. *J. Immunol.* **172**, 2731–2738 (2004).
77. Gupta, S. et al. Sex differences in neutrophil biology modulate response to type I interferons and immunometabolism. *Proc. Natl. Acad. Sci.* **117**, 16481–16491 (2020).
78. Ovadia S., Özcan A., Hidalgo A. The circadian neutrophil, inside-out. *J. Leukoc. Biol.* **113**, 555–566 (2023).
79. Thasneem, Y., Sajeesh, S. & Sharma, C. P. Effect of thiol functionalization on the hemo-compatibility of PLGA nanoparticles. *J. Biomed. Mater. Res. Part A* **99**, 607–617 (2011).
80. Moriceau, S., Lenoir, G. & Witko-Sarsat, V. In cystic fibrosis homozygotes and heterozygotes, neutrophil apoptosis is delayed and modulated by diamide or roscovitine: evidence for an innate neutrophil disturbance. *J. Innate Immun.* **2**, 260–266 (2010).
81. Leitch, A. et al. Cyclin-dependent kinases 7 and 9 specifically regulate neutrophil transcription and their inhibition drives apoptosis to promote resolution of inflammation. *Cell Death Differ.* **19**, 1950–1961 (2012).
82. Leitch, A. E. et al. The cyclin-dependent kinase inhibitor R-roscovitine down-regulates Mcl-1 to override pro-inflammatory signalling and drive neutrophil apoptosis. *Eur. J. Immunol.* **40**, 1127–1138 (2010).
83. Siebert, S. et al. Targeting the rheumatoid arthritis synovial fibroblast via cyclin dependent kinase inhibition: an early phase trial. *Medicine* **99**, e20458 (2020).
84. Center C.-S. M. Multicenter study of seliciclib (R-roscovitine) for cushing disease) https://ClinicalTrials.gov/show/NCT03774446 (2018).
85. Volchuk, A., Ye, A., Chi, L., Steinberg, B. E. & Goldenberg, N. M. Indirect regulation of HMGB1 release by gasdermin D. *Nat. Commun.* **11**, 4561 (2020).
86. Barnett-Vanes, A., Sharrock, A., Birrell, M. A. & Rankin, S. A single 9-colour flow cytometric method to characterise major leukocyte populations in the rat: validation in a model of LPS-induced pulmonary inflammation. *PLoS One* **11**, e0142520 (2016).

Acknowledgements

This study was supported by the National Research Foundation of Korea (RS-2024-00354235, recipient B.S.K., and NRF-2022R1A2C2009067, recipient H.J.P.) funded by the Ministry of Science and ICT, Republic of Korea.

Author contributions

C.K. and B.S.K. conceived the work. C.K. and H.K. designed the experiments. C.K., H.K., and W.S.S. performed the experiments. M.J., J.H., S.M., J.H.P., J.J.K., M.K., S.K., K.B., M.J.K., H.J.P., and B.S.K. provided intellectual input. C.K., H.K., H.J.P., and B.S.K. wrote the manuscript. C.K., H.K., M.J., W.S.S., and B.S.K. prepared the figures. H.J.P. and B.S.K. supervised all aspects of the research.

Competing interests

The authors declare no competing interests.

Additional information

Supplementary information The online version contains supplementary material available at https://doi.org/10.1038/s41467-024-52812-6.

Correspondence and requests for materials should be addressed to Hun-Jun Park or Byung-Soo Kim.

Peer review information *Nature Communications* thanks Xiao Luo, and the other, anonymous, reviewer(s) for their contribution to the peer review of this work. A peer review file is available.